Journal of Hydrology 564 (2018) 133–148

Contents lists available at ScienceDirect

Journal of Hydrology

journal homepage: www.elsevier.com/locate/jhydrol

Research papers

On the resilience of small-island freshwater lenses: Evidence of the long-term impacts of groundwater abstraction on Bonriki Island, Kiribati

Vincent E.A. Post[a,b], Amandine L. Bosserelle[c], Sandra C. Galvis[a,c,d], Peter J. Sinclair[c], Adrian D. Werner[a,*]

[a] College of Science and Engineering and National Centre for Groundwater Research and Training, Flinders University, Adelaide, Australia
[b] Federal Institute for Geosciences and Natural Resources (BGR), Stilleweg 2, Germany[1]
[c] Pacific Community – Geoscience Energy, and Maritime Division, Suva, Fiji
[d] Deltares, Utrecht, The Netherlands[1]

ARTICLE INFO

This manuscript was handled by Corrado Corradini, Editor-in-Chief, with the assistance of Brian D. Smerdon, Associate Editor

Keywords:
Fresh groundwater lens
Salinity
Small islands
Kiribati
Atoll island
Water management

ABSTRACT

Groundwater on islands occurs in the form of freshwater lenses that serve as an important water resource for local inhabitants. These lenses are highly vulnerable to salinization due to natural recharge variations and groundwater abstraction. Determining the sustainable yield from freshwater lenses is challenging because the lens response during drought periods and the long-term effects of pumping are both difficult to predict. The exceptionally detailed and long data record for Bonriki Island of the Tarawa atoll (Kiribati) made it possible to develop a three-dimensional variable-density model of the island. Field data and modelling results highlight the strong control of rainfall variability and pumping on the temporal dynamics of the freshwater lens. The model reproduces the salinity observations in both monitoring and pumping wells reasonably well, and provides a rare example of physically based island simulation based on an extensive data set. It enables the analysis of freshwater volume and fluxes of submarine groundwater discharge, which is impossible based on the field observations alone. Under natural as well as abstraction conditions, submarine groundwater discharge responds rapidly and almost proportionally to recharge. Theoretical model scenarios with scaled abstraction rates show that lens contraction caused by pumping is a nearly linear function of the total pumped volume, whereby the abstraction rate and the timing of depletion are approximately inversely proportional. Modelling indicates that when monthly recharge inputs fall below around 2500 m^3/d (i.e., a flux of 1.7 mm/d) plus the abstraction rate, the lens tends to contract. Thus, despite the highly distributed and extensive abstraction network on Bonriki Island, a significant amount of recharge is eventually lost to submarine groundwater discharge. The long-term freshwater storage trend indicates that Bonriki Island's lens is still contracting after 27.5 years of pumping, and lens thinning is threatening to impact the water supply salinity. This means that even permeable, small islands like Bonriki may take at least two decades to realise new equilibrium conditions that reflect pumping stresses, which is an important consideration in assessing the sustainable yield of small islands, in particular those less resilient to pumping than Bonriki.

1. Introduction

Water resource availability and sustainable management practices are recurring issues on islands, in particular for the Small Island Developing States (SIDS), a group of 52 developing countries on low-lying carbonate and volcanic islands that share similar sustainable development challenges (UNESCO, 2016). The SIDS are faced with the need to secure reliable freshwater supplies despite increased climate variability, sea-level rise, and, in many locations, population growth (White and Falkland, 2012; Allen et al., 2014). On small islands, rainwater and groundwater are the primary natural sources of water supply (Illangasekare et al., 2006; Liu et al., 2006). Groundwater on islands occurs in the form of freshwater lenses, which necessitates a special form of management to mitigate the risk of salinization and other forms of anthropogenic contamination (Bailey et al., 2010; White and Falkland, 2010).

Atoll and similar coral-reef islands represent a specific subgroup of the broader category of small islands, and have many common

* Corresponding author at: College of Science and Engineering, Flinders University, GPO Box 2100, Adelaide, SA 5001, Australia.
E-mail address: adrian.werner@flinders.edu.au (A.D. Werner).
[1] Present affiliation.

https://doi.org/10.1016/j.jhydrol.2018.06.015
Received 19 January 2018; Received in revised form 29 May 2018; Accepted 5 June 2018
Available online 15 June 2018

characteristics and management problems (Falkland, 1991). The volume of freshwater stored within an atoll island depends on the balance between recharge from rainfall, and losses through evapotranspiration, discharge into the ocean and lagoon, mixing with underlying seawater, and groundwater abstraction for human use. Determination of the sustainable yield requires that these processes can be quantified, including the transient nature of rainfall and the recharge generated from it. In particular, the response of the freshwater lens to droughts must be known, as groundwater during these times becomes the primary or even the sole source of water supply (White and Falkland, 2010; Werner et al., 2017).

Previous studies have shown that freshwater lenses respond to recharge events at timescales ranging from hours to months. For example, Jones et al. (2004) determined the response of a borehole salinity profile on Grand Cayman Island to a heavy rainfall event and found that salinities decreased across the entire 12-m profile as early as 1.5 h after the storm. Lens behaviour over longer time-scales, for example in response to intra- and inter-annual variations in rainfall, has been widely studied. Woodroffe and Falkland (2004) showed how the base of the freshwater lens responded to recharge variation over an eight-year period for two study sites in the Cocos (Keeling) Islands. They found that where the lens is bounded by the unconformity between Holocene sediments and Pleistocene limestone, found at a maximum depth of 15 m below the ground surface, fluctuations of the base of the lens with recharge tend to be more subdued than when the freshwater is contained principally within the Holocene sediments. Nonetheless, the effects of droughts lasting up to several months resulted in significant thinning of the lens in both cases.

Van der Velde et al. (2006) found that the salinity of pumped freshwater on the island of Tongatapu (Tonga) fluctuated around its mean value in response to the El Niño-Southern Oscillation (ENSO), and that the Southern Oscillation Index (SOI) could be used to predict groundwater salinity with a lag time of 10 months. They applied a time-series model that was fitted to observed data by parameter optimization. The method sometimes yielded parameter combinations representative of unrealistically long transit times between the point of infiltration and the well (Van der Velde et al., 2007).

The response of small island freshwater lenses to changes in recharge has also been investigated using numerical models. Early studies (Underwood et al., 1992; Griggs and Peterson, 1993) showed that, as expected, the lens will decrease in thickness in response to a reduction in recharge. Comte et al. (2014) highlighted the importance of vegetation, which through its influence on groundwater recharge, may exert a strong control on the thickness of the lens. They found that reduced recharge due to transpiration promotes seawater intrusion, but a feedback mechanism exists because the increased salinity affects the health of the vegetation, which reduces transpiration and thus enhances recharge. Bailey et al. (2014) used numerical simulations to infer the effect of variable rainfall on the thickness of freshwater lenses for atoll islands of the Maldives. Their results showed that variations in lens thickness of up to 50% can occur, but their simulations did not consider pumping, and the hydraulic parameters were not varied between different islands. A comprehensive, calibrated model of Home Island, part of the Cocos (Keeling) Islands, was produced by Ghassemi et al. (2000). The study highlighted the complications of modelling atoll island environments, and the need for incorporation of system stresses at a temporal resolution of one month or less in order to capture the transient nature of the observed salinity variations. Based on a poor fit between model outcomes and field data, the authors drew pessimistic conclusions about our capacity to model freshwater lens dynamics, even if abundant field data are available. Holding and Allen (2015) assessed the impact of reduced recharge due to climate change for Andros Island in the Bahamas using a three-dimensional model and concluded that this could lead to a loss of freshwater volume of up to 19%.

While the role of climate-driven recharge variability in controlling lens behaviour has been well studied, there are fewer investigations into the effect of pumping on lens dynamics, in particular where historical trends and spatial variability in pumping are known and accounted for. Griggs and Peterson (1993) conducted two-dimensional numerical simulations of the freshwater lens for the Laura area of the Majuro Atoll in the Marshall Islands. They concluded that the sustainable yield is almost twice as high when infiltration galleries instead of vertical wells are used to abstract groundwater. Moreover, they reported that for simulations with monthly averaged recharge, a higher sustainable extraction was found than for yearly averaged recharge, and that significant quantities of water could be abstracted from the lens during sustained periods of drought. Their simulations spanned a period of 3 years only though, and were therefore not inclusive of multi-decadal trends.

A need therefore remains for long-term studies that investigate the combined effects of rainfall variability, pumping and physical groundwater processes to better understand the resilience of island freshwater lenses against droughts, and to guide management of the freshwater lens to ensure the supply of suitable quality water. The multi-decadal impact of abstraction on the freshwater volume in particular has not been investigated in detail previously, even though this is crucial to the long-term sustainability of island water supply systems. Furthermore, Werner et al. (2017) call for the continued use of data from established and long-running sites such as Bonriki (Kiribati) or Cocos (Keeling) Islands, to develop exemplar investigations to inform groundwater management, accounting for the specific conditions of individual atoll island settings.

Here, we present a study of the freshwater lens on the island of Bonriki, South Tarawa, Kiribati. ENSO cycles have a direct impact on the recharge to groundwater on the atoll (Australian Bureau of Meteorology and CSIRO, 2011). The detailed long-term monitoring data that have been collected for more than three decades provide a unique case study of lens behaviour under the influence of variable recharge and increased pumping stress. The dataset includes measurements of groundwater salinity, rainfall and evaporation, pumping records, and pumped water salinity (Sinclair et al., 2015). In terms of size, measured by its maximum width (0.95 km), Bonriki is one of the larger islands in the Pacific, with 86% of 1035 islands > 0.25 km being smaller (Stewart et al., 2014). Its geology (i.e., thickness of the Holocene sediment, sediments changing from coral fragments on the ocean side to fine sand on the lagoon side) and rainfall amount (just like 886 out of 1035 islands > 0.25 km, Bonriki falls in the > 1500 mm/year category of Stewart et al., 2014) are comparable to other islands.

The objective of the present study is to quantify the effect of recharge and abstraction on the freshwater lens of Bonriki Island, because it is an exemplar system of dual-aquifer carbonate islands worldwide (Werner et al., 2017). Dual-aquifer carbonate islands are those in which Holocene sands with a relatively low hydraulic conductivity overly more permeable Pleistocene reef deposits (Vacher, 2004). Examples of similar islands include those in the Majuro Atoll (Marshall Islands), the Cocos (Keeling) Islands, Diego Garcia Atoll, as well as the Lower Florida Keys and the Bahamas. A numerical model of variable-density flow and solute transport was calibrated to reduce discrepancies between modelled and observed groundwater salinities. The model was subsequently used to quantify the volumes and fluxes of fresh- and saltwater to determine the long-term fate of the freshwater lens. Following a similar approach to Van Loon and Van Lanen (2013) and Knowling et al. (2015), except in our case the model is a density-dependent lens simulator, the model was run for both natural and anthropogenic conditions to allow for the distinction of the impact of pumping from lens growth and shrinkage due to natural variations in recharge.

2. Study area

The study area is the Bonriki Water Reserve (Latitude 1°23′10″ N, Longitude 173°8′50″ E), which forms part of the Tarawa atoll in

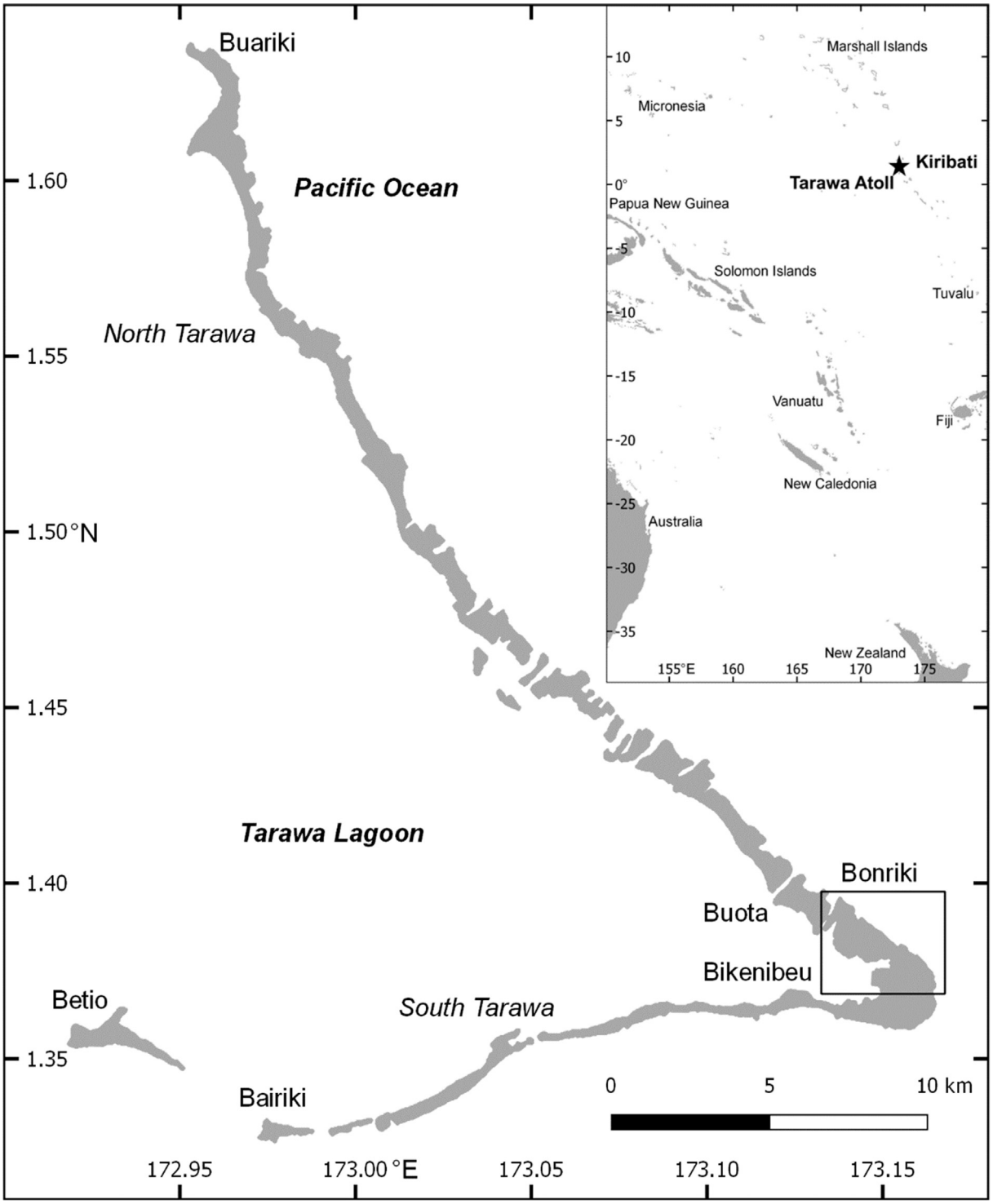

Fig. 1. Map showing the location of the Tarawa Atoll. The black solid rectangle in the main figure outlines the location of the map shown in Fig. 2.

Western Kiribati (Fig. 1) in the Pacific region. Besides the Bonriki freshwater lens, the atoll's National Water Reserve includes the lens of Buota Island. The lenses are the primary supply for the more than 56,000 residents (2015 census) of South Tarawa (KNSO, 2016), which experienced an annual 2.3% population growth rate between 2010 and 2015. The reticulated water system extends from Buota and Bonriki Islands to some 30 km to the western island of Betio (Fig. 1), and provides potable water to at least 67% of South Tarawa's population.

The topography is flat and the elevation of the land surface is generally between 2 and 4 m above mean sea level. Fig. 2 presents an aerial depiction of the island, with key water infrastructure labelled. A water treatment plant and Bonriki International Airport are located centrally above the Bonriki lens, while residential areas occur around the lens fringes. Extensive vegetation, primarily coconut trees, otherwise covers the lens area. The study area is bounded to the northeast by a tidal channel and a beach on a rock platform from which a reef flat extends into the ocean. On the western side is the atoll's lagoon, in which open water and sand flats with stands of mangrove alternate. Inland lakes occur in the northwestern corner of the reserve ("Wetlands" in Fig. 2). An aquaculture facility has been constructed to the

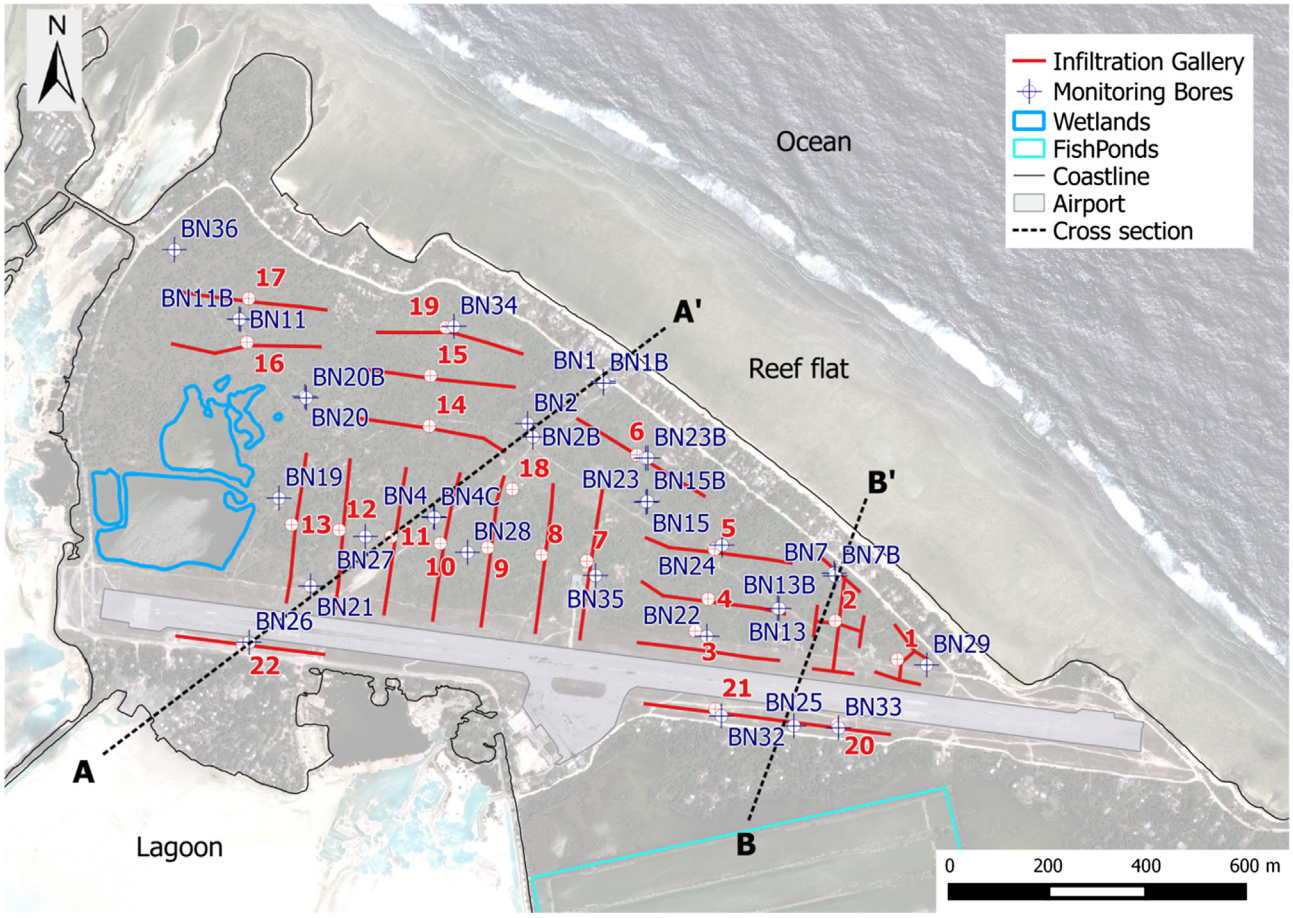

Fig. 2. Map showing the Bonriki Water Reserve, horizontal collector wells (known as infiltration galleries) with pumping station structures located in the centre of each gallery, and monitoring bore locations. The blue lines in the western region of the island indicate the location of inland lakes. AA′ and BB′ identify cross sections shown in later figures. The elevation of the terrain where galleries 9–13 are located is lower by about 1 m on average compared to where the other galleries north of the runway are. See Fig. 1 for map location.

south of the water reserve, as indicated by approximately east-west oriented saltwater ponds in Fig. 2.

Tarawa atoll is located in the hot, humid tropical zone that extends over much of the equatorial Pacific Ocean, and is influenced by the southeast trade winds for most of the year (Falkland, 1992; Falkland and Woodroffe, 2004). It is outside the area of cyclonic activity, and ENSO cycles strongly affect the climate and, in particular, the rainfall (Burgess, 1987). The Southern Oscillation Index and Tarawa's annual rainfall are strongly correlated (White et al., 2007). Daily rainfall data are available from the meteorological station on Betio from 1947 to the present. The dry season generally occurs from May to November, while the wet season is from December to April. The average annual rainfall at Betio from January 1947 to December 2013 was 1998 mm. Daily rainfall has also been recorded at Bonriki Airport since 2009. The rainfall on Bonriki is, on average, 6% less than that on Betio (Galvis-Rodriguez et al., 2017). Falkland (1992) estimated the potential evapotranspiration at the Betio station from average monthly pan evaporation data measured between 1981 and 1991. The mean pan evaporation rate was 6.15 mm/d, with a minimum of 5.5 mm/d in July and a maximum of 6.9 mm/d in September and October.

Thirty-six boreholes have been drilled on Bonriki (Sinclair et al., 2015). Geological profiles based on lithological descriptions of samples from these boreholes show that the subsurface can be divided into a Holocene and an underlying Pleistocene unit, as illustrated in Fig. 3. The Pleistocene limestone comprises skeletal wackestones and packstones that are sometimes fractured (Dunham, 1962; Jacobson and Taylor, 1981). Karstification of the limestone occurred during sea level lowstands in glacial periods, and consequently the topography of the limestone's palaeo-surface is highly irregular. Limestone occurs at an elevation between approximately 12 m and 20 m below mean sea level and is unconformably covered by Holocene granular deposits (Falkland and Woodroffe, 2004; Jacobson and Taylor, 1981). The latter consist of (i) unconsolidated sand and gravel near the lagoon, (ii) poorly cemented hard coral fragments inland, and (iii) consolidated coral deposits at depth and towards the ocean side (Fig. 3).

There is a pronounced demarcation between the hydraulic properties of the Holocene and Pleistocene units of Bonriki Island (Falkland and Woodroffe, 2004). The hydraulic conductivity (K) of the Holocene sediments varies from 5 to 20 m/d, whereas the K of the Pleistocene limestone tends to increase with depth. It ranges between $10 < K < 20$ m/d near the boundary with the Holocene sediments, to $K > 100$ m/d at greater depth (Falkland and Woodroffe, 2004; Jacobson and Taylor, 1981).

The salinity monitoring network on Bonriki currently consists of 23 boreholes equipped with multi-level observation wells (Fig. 2), but this number has varied in time (Sinclair et al., 2015). Measurements of electrical conductivity (EC) from these wells are available from as early as 1980, although the bulk of the data was collected after the year 2000. The measurements have demonstrated the existence of fresh to brackish groundwater up to 25 m deep (Falkland, 1992; Sinclair et al., 2015), as illustrated by the EC contour lines in the cross sections of Fig. 3. The high K of the Pleistocene limestone enhances the mixing of freshwater and seawater, and consequently a broad transition zone exists in this unit (Jacobson and Taylor, 1981; White et al., 2008). The

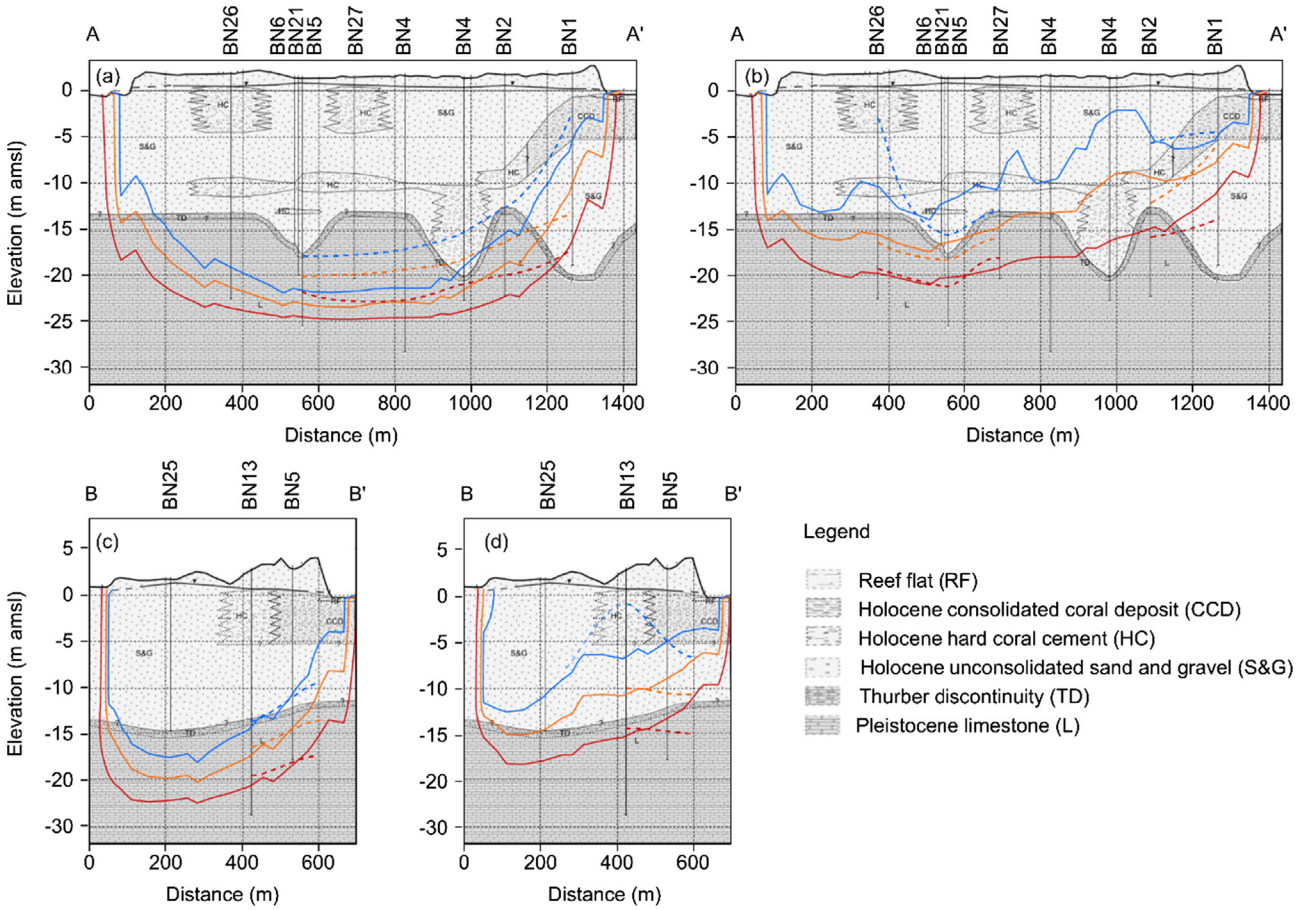

Fig. 3. Cross sections showing the lithology, water table elevation and freshwater lens geometry for (a) May 1985 along profile line A-A′, (b) June 2014 along profile line A-A′, (c) May 1985 along profile line B-B', (d) June 2014 along profile line B-B′. Cross section locations are shown in Fig. 2. The dashed lines represent electrical conductivity (EC) contours of 2.5, 10 and 25 mS/cm (blue, orange and red colours, respectively) based on interpolation of field measurements. Solid lines are obtained from the numerical model (see Section 3). The EC contour values correspond to a TDS of 1.8, 7.2 and 18 g/L, respectively, and were adopted for consistency with previous publications (e.g., Falkland and Woodroffe, 2004). (For interpretation of the references to colour in this figure legend, the reader is referred to the web version of this article.)

high rate of mixing in the Pleistocene limestone largely restricts the presence of potable freshwater to the Holocene strata (Sinclair et al., 2015).

Fig. 2 shows the location of the 21 currently operating horizontal collector wells, commonly referred to as infiltration galleries. Utilization of the lens started at rates less than 100 m^3/d in the mid-1970s with the installation of the first infiltration galleries (Mather, 1973; Wagner, 1977). Since then, estimates of the sustainable yield have been updated a number of times, and the capacity of the water supply system has expanded. The chronology of the studies and the annual volumes of groundwater abstracted are summarised in Fig. 4.

The water table occurs at up to 1.5 m above mean sea level (Sinclair et al., 2015). Fluctuations of the water table of up to 0.5 m occur in response to the tide in the lagoon and ocean, making it difficult to ascertain long-term water-level trends from manual readings. Due to the heterogeneous nature of the subsurface, the tidal fluctuations do not follow a systematic spatial pattern, which is generally the case for atoll islands (White and Falkland, 2010).

3. Numerical model

3.1. Model setup

SEAWAT Version 4 (Langevin et al., 2008) was used to develop a transient flow and solute transport model. SEAWAT couples MODFLOW and MT3DMS to simulate variable-density groundwater flow and solute transport, and has been verified and used widely for simulating seawater intrusion. The conceptual model for the numerical groundwater model was based on all aforementioned hydrogeological information and is depicted as a three-dimensional block diagram in Fig. 5. The diagram includes a simplified geological setting and shows the dual nature of the aquifer system that results from the Holocene sediments overlaying the Pleistocene karstified limestone.

A transient model simulation was set up for the period 1 January 1948 to 30 June 2014 using monthly stress periods (798 in total). The model covers an area of about 9.5 km^2 and extends from the fishponds in the southeast, to the channel between Bonriki and Buota in the west. An aerial view of the model grid is given in Fig. 6. The model domain has a width of 2.8 km between the lagoon and the ocean (northeast to southwest) and a length of 3.4 km in a southeast to northwest direction. Below the ocean and the lagoon, the model extends offshore to a distance of at least 100 m from the shoreline to minimize the influence of the aquifer truncation at the lateral boundaries on the prediction of the lens behaviour. The finite-difference grid was rotated in order to minimize the number of cells. The model had 33 rows, 52 columns and 36 layers, with 58,678 active cells. The layer thickness varied between 0.5 m for layer two, to 25 m for the three deepest layers. The thickness of the first layer varied according to the surface topography. Table S1 of the electronic Supplementary material (ESM) presents additional key metrics of the model's discretization.

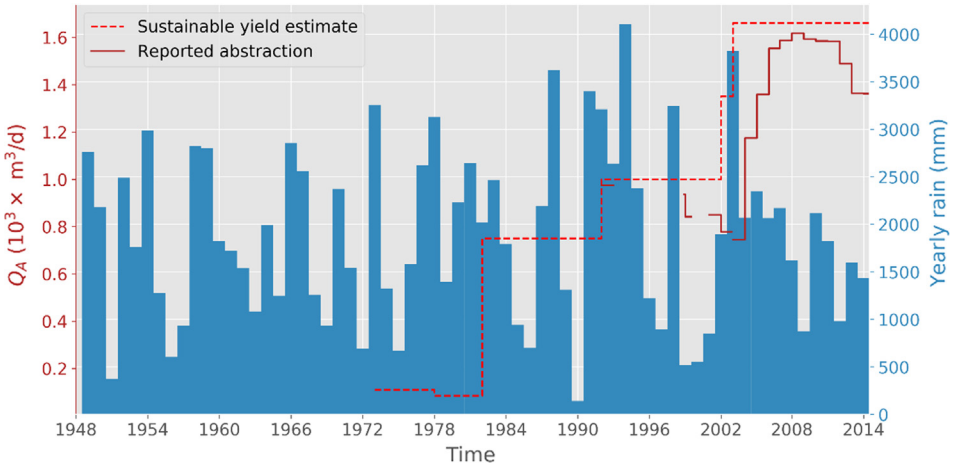

Fig. 4. Overview of pumping rates and published sustainable yield estimates for the Bonriki lens, according to Mather (1973), AGDHC (1982), Falkland (1992), Alam et al. (2002), White et al. (2002), White et al. (2008), and Sinclair et al. (2015). The recorded abstraction rates are annual averages based on Kiribati's Public Utilities Board (PUB) data unless otherwise indicated. Corrections were applied to the reported abstraction rates from 2004 onward as detailed in Section 3.2.2.

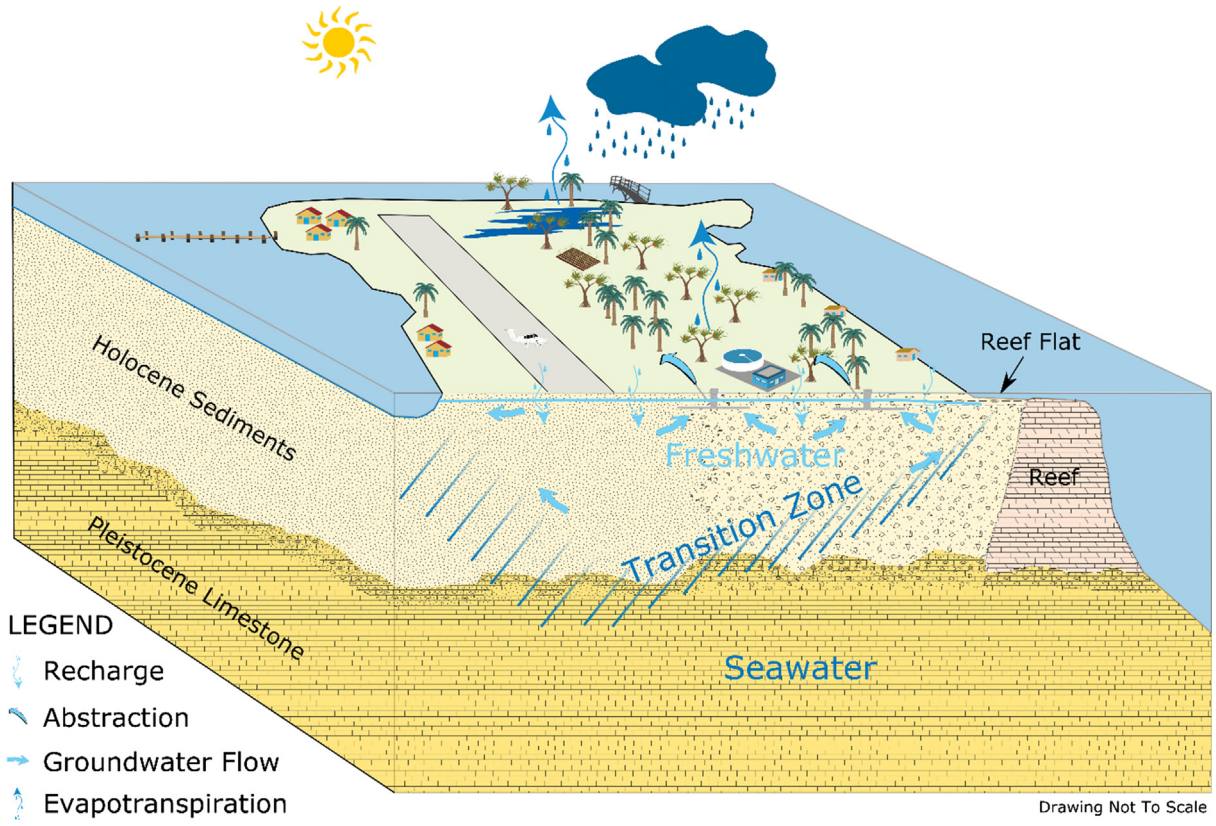

Fig. 5. Conceptual three-dimensional block diagram of the Bonriki groundwater system, modified from Bosserelle et al. (2015). Coarser sediments encountered in the region closest to the ocean (right-hand) boundary are illustrated by the pattern change within the Holocene layer. Symbols courtesy of the Integration and Application Network, University of Maryland Center for Environmental Science (ian.umces.edu/symbols/).

3.2. Boundary conditions and stresses

3.2.1. Boundary conditions

Specified heads were assigned to cells that sit below the ocean (reef flat and/or reef slope) or the lagoon (depending on the bathymetry). Cells of which the centre node was elevated above the ocean or lagoon floor were made inactive, and only the cells in the first active layer were assigned specified heads, except at the outer boundaries of the model grid where the heads were specified in all active model layers. A salt-water head equal to mean sea level was assigned to all of the specified-head cells. The concentration of the specified-head cells was allowed to vary during the simulations. Groundwater exiting the active region of the model domain carried the model-calculated salt content of a boundary cell, whereas water entering into the active domain was assigned the total dissolved solids (TDS) concentration of seawater. Specified-head cells were also assigned to the cells in model Layer 1 in the fish ponds area (see Fig. 6).

Cells in the topmost layer on the island were assigned a specified flux that varied in time depending on the calculated recharge rate (see Section 3.2.1). The TDS concentration of the recharge was made dependent on the recharge rate to allow for the effect of evapotranspiration on the solute concentrations. For recharge rates higher than 100 mm/month, the recharge TDS was 0.31 kg/m^3, between 50 and 100 mm/month the TDS was 0.38 kg/m^3, and between 0 and 50 mm/month the TDS was 0.45 kg/m^3. Recharge TDS values were set to accord with shallow groundwater salinities, and taking into account

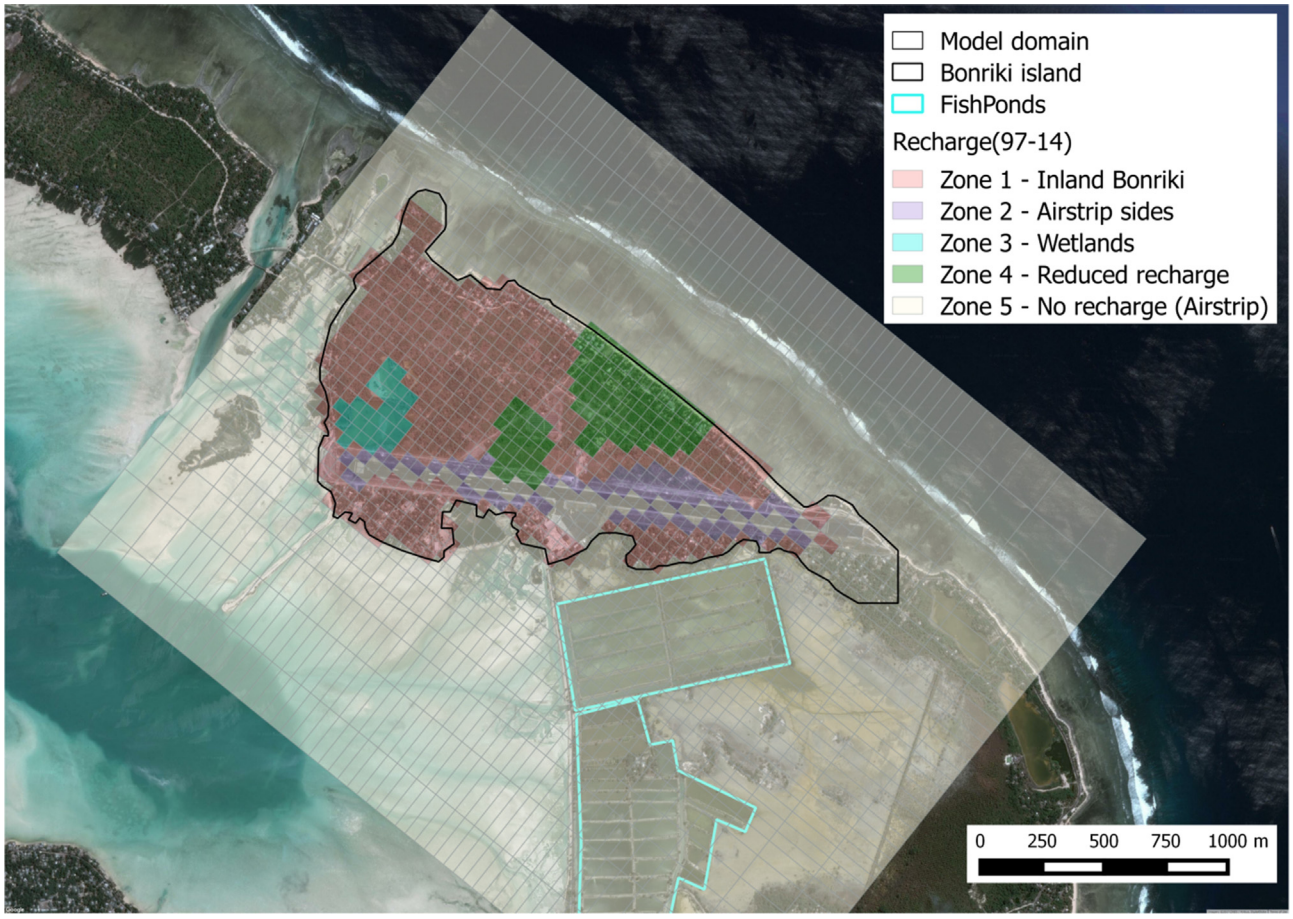

Fig. 6. Map showing the outline of the finite-difference grid and the distribution of recharge zones across Bonriki Island.

the higher evapo-concentration of lower recharge rates.

3.2.2. Groundwater recharge

The recharge was estimated using the water balance model WATBAL (Falkland, 1992; Falkland and Woodroffe, 2004). The program uses input time series of daily rainfall and evaporation, and solves the following equation:

$$R = P - E - \Delta V \quad (1)$$

where R is recharge, P is rainfall, E is evapotranspiration, and ΔV is the change in storage within the soil moisture zone. All quantities are expressed in units of mm/d. Surface runoff was neglected because of the high infiltration capacity of the soils, the flat topography and the lack of surface flow features on the island. The evapotranspiration term includes evaporation from the soil surface, transpiration by vegetation (including from both soil water and groundwater), and the interception of rainfall by tree canopies. Other features of the code are described by Falkland (1992), Alam et al. (2002), and Falkland and Woodroffe (2004). For the input time series of P, the rainfall on Bonriki was used in this study (see Fig. S1 of the ESM), which, applying the aforementioned 6% correction factor, was determined from the rainfall measured at Betio between 1947 and 2009. For the period 2009 – June 2014, the measured values at Bonriki were used. The evaporation was based on the monthly pan evaporation values reported by Falkland (1992). Other input parameters for the WATBAL code are listed in Table S2 of the ESM.

Daily net recharge values from WATBAL modelling were aggregated into monthly totals for use in the groundwater model. The average recharge produced by WATBAL was approximately 57% of the mean rainfall rate of 1887 mm/year. This can be compared to an estimated 11% of 847 mm/year for Kiribati's Christmas Island for the same degree of coconut tree cover, but Falkland and Woodroffe (2004) considered this value to be an underestimate since monthly rainfall averages were used instead of daily values. Percentages for three of the Cocos (Keeling) Islands, were calculated to be 29%, 44% and 49% of 1950 mm/year of rainfall for a coconut tree land cover fraction of 0.8, 0.15 and 0, respectively, for the period 1953–1993 (Falkland and Woodroffe, 2004). For this case, the difference with Bonriki Island is mainly due to a higher soil zone thickness in the model of the Cocos (Keeling) Islands (500 mm vs the 300 mm adopted for our study), with our WATBAL parameters arguably being well-constrained by detailed recharge studies conducted at Bonriki by White et al. (2002).

On average, evapotranspiration losses were partitioned into canopy interception (8% of rainfall) and evapotranspiration from shallow- and deep-rooted vegetation (32% and 3% of rainfall, respectively). Recharge was applied in the spatially distributed zones shown in Fig. 6. The values directly from the WATBAL model were used across most of the island (zone 1; Fig. 6), whereas modifications were made for hydrogeological features in some areas that were not included in WATBAL calculations. For example, no recharge was applied to cells beneath the airstrip (zone 5), while the cells adjacent to it were assigned a 50% higher recharge to account for the runoff from the tarmac (zone 2). In zone 4, recharge was 40% lower than the WATBAL values to account for the presence of the reef flat rock, which is thought to restrict recharge to the more permeable Holocene sediments, in combination with the higher density of deep-rooted vegetation that are thought to tap directly into the groundwater (Galvis-Rodriguez et al., 2017; Sinclair et al., 2015). In this zone, a subdued response of the water level to rainfall was observed in comparison to the other parts of the lens reserve (Sinclair et al., 2015). No recharge was applied where there is

open water (i.e., ocean, lagoon, fish ponds; see Fig. 6), except at the wetlands (zone 3), where the recharge rate was calculated as the rainfall minus the open water evaporation rate, which was calculated by taking the pan evaporation values Falkland (1992) multiplied by 0.7. Negative recharge can occur during dry months in all zones except zone 5. In the wetlands (zone 3), this occurs when evaporation exceeds precipitation, while in zones 1, 2 and 4, this occurs when groundwater usage by deep-rooted vegetation exceeds the recharge to the water table from the soil zone.

3.2.3. Groundwater abstraction

Abstraction rates have been recorded regularly by Kiribati's Public Utilities Board (PUB) since 1998. During the present study, it was found that the flowmeters that were used to monitor the abstraction rates since 2004 were overestimating the abstracted volume due to improper installation. Based on a validation of the flowmeters in 2015, it was estimated that the actual flow rate is 18% lower than the recorded rates at the main trunk feeding into the water treatment plant (Loco, 2017). The overestimation of flow rates at individual galleries was estimated to range from 6.5% at gallery 13 to 42.1% at gallery 21. Based on these findings, the recorded flow rates were adjusted (revised rates are given in Fig. 4). In what follows, reference to abstraction rates implies the corrected values.

The infiltration galleries were implemented in the model by assigning abstraction rates to the cells in the uppermost layer of the model grid that coincide with the location of the galleries. Monthly abstraction rates were assigned based on the values reported by PUB, corrected for the aforementioned flowmeter discrepancies. The reported total abstraction rate for each well was equally apportioned to the model cells by dividing it by the number of cells that represent an infiltration gallery. No measured abstraction rates are available for the period January 1987 to November 1998, and only a best estimate can be adopted based on published reports (e.g., Falkland, 1992). Therefore, a constant abstraction rate of 850 m^3/day was used in the model distributed between the 18 galleries existing at the time. Pumping rates were less than 100 m^3/d before 1987, and since no detailed information about this period exists and the abstraction rates are small, no pumping was simulated in the model prior to January 1987.

To ascertain the degree to which changes in the freshwater lens volume are due to abstraction of groundwater or due to the rainfall conditions, a model without groundwater abstraction was run. More precisely, in the model without abstraction, pumping rates were reduced by a factor of 1000 so that the salinities at the pumping galleries could still be easily evaluated and compared to the model with abstraction. In addition, simulations with scaled abstraction rates, with otherwise the same stresses and parameters, were run to evaluate the long-term behaviour of the lens under reduced rates of groundwater withdrawal. Specifically, we sought to explore the level of pumping at which the lens would recover to "natural conditions" (i.e., in the absence of pumping) during high rainfall periods. Three additional scenarios were considered in which scaled abstraction rates were 75%, 50% and 25% of the abstraction rates used in the calibration simulation (i.e., as listed in Fig. 4).

3.3. Model calibration

The total simulation time was subdivided into a calibration period subsequent to 1 January 1997, and a validation period from 1 January 1948 to 31 December 1996. Calibrated parameters were the horizontal and vertical hydraulic conductivities (K_H, K_V), porosity (n), and dispersivity (horizontal longitudinal, α_L; vertical longitudinal, α_V; and transverse, α_T). Unique K_H and K_V values were assigned to the Holocene sediments, and upper and lower Pleistocene layers, whereas n and {α_L, α_T, α_V} were the same for all layers. Previous studies (e.g., Alam et al., 2002) that employed two-dimensional cross-sectional models provided initial estimates of these parameters. Calibration was undertaken using manual trial-and-error due to the run-times (around 3.5 h).

The initial heads and concentrations for the transient model were determined from the heads and concentrations after the final time step of the model with the updated calibration parameters but without abstraction. Since no data are available at the model starting time (1 January 1948) and no information is available about the antecedent recharge rates, this is a somewhat arbitrary modelling choice. However, given the high permeability and small scale of the model, the initial conditions have little effect on the final outcome for the period of main interest, i.e., the post-1986 abstraction period.

EC values were available at the 22 multi-level monitoring wells and for the 22 abstraction galleries, totalling 6708 salinity data points during the calibration period. Measurement of the EC of abstraction galleries started in 1977, but regular readings from individual galleries have only been available since 2006. The EC of the water from the treatment plant, representing the mixed water from all the galleries before it is fed into the trunk main pipeline, is also available. For comparison with the modelled TDS concentrations, the measured EC values (in units of mS/cm) were converted to TDS (in units of kg/m^3) by multiplying by 0.72. The EC-TDS conversion was obtained from comparison between EC and TDS where water chemistry data were available (Galvis-Rodriguez et al., 2017). The concentrations of the multi-level observation wells were compared to the model-calculated concentrations in the cells corresponding to the location and depth of the measurement point. The modelled concentrations of the cells corresponding to the abstraction galleries were used to calculate a flux-weighted average concentration, which could be compared to the measured values of the abstracted water from each gallery, and from all galleries combined.

3.4. Output variables

The modelled concentrations were used to determine the volume of the freshwater lens, V_f, which was calculated by summing the saturated volume of all model cells in which the electrical conductivity was less than 2.5 mS/cm at the end of each stress period. The difference between the modelled freshwater lens volume without abstraction ($V_{f,na}$) and with abstraction ($V_{f,a}$) was $\Delta V_f = V_{f,na} - V_{f,a}$. The difference between the freshwater volume between two consecutive stress periods was $\Delta V'_f = V_{f,sp} - V_{f,sp-1}$, where sp in the subscript indicates the stress period number. Note that $\Delta V'_f$ is positive/negative when the lens is growing/shrinking.

The total abstracted volume of groundwater since the start of pumping on 1 January 1987 was defined as

$$V_{abs,tot} = \sum_{1}^{N} Q_{A,i} \Delta t_i \tag{2}$$

where $Q_{A,i}$ is the volumetric abstraction rate for month i (m^3/d) and Δt_i is the length of month i in days ($28 \le \Delta t_i \le 31$). The total number of months in the simulation was $N = 798$.

The model results were compared to the 12-month percentile rainfall ranking (R_{12}), which is used as a drought index in Kiribati's water management and drought response plans (e.g., White et al., 2008). R_{12} was calculated for each month by first summing the month's rainfall and that of the preceding 11 months. This summed total was then ranked relative to other 12-month sums that include the same month-sequence (e.g., February-to-January, May-to-April, October-to-September, etc.) within the simulation period (January 1948 – June 2014). Thus, an R_{12} value of 100% means that the previous 12 months were wetter than any other 12-month period with the same start and end months.

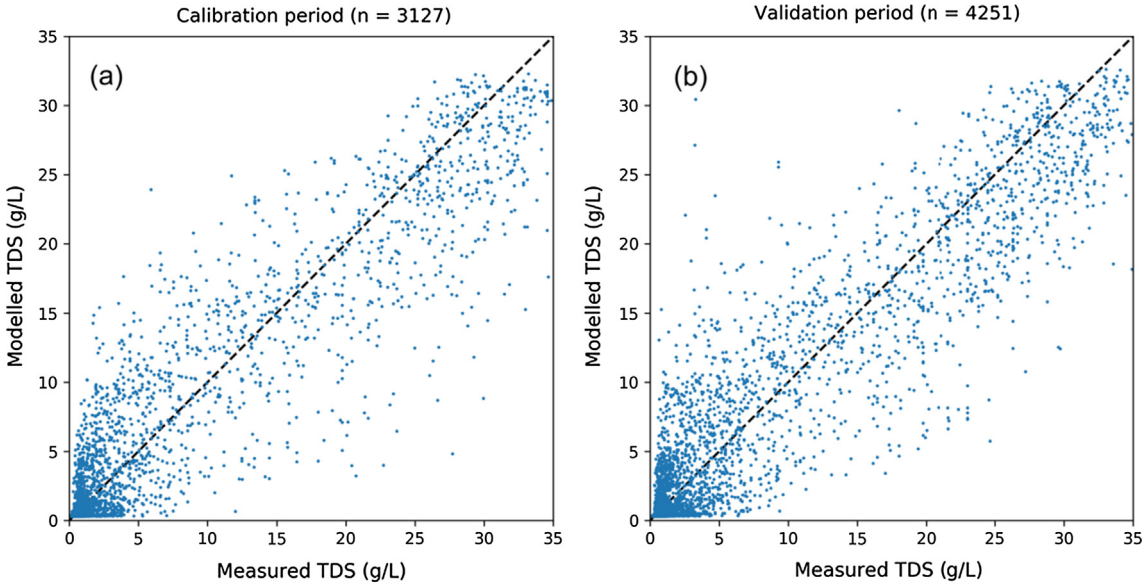

Fig. 7. Modelled versus observed concentrations for (a) the calibration period 1997–2014 and (b) the validation period 1948–1996.

4. Results

4.1. Calibration results

Fig. 7 shows the comparison of the salinities of the multi-level observation wells with the modelled salinities for the calibration and validation periods. The final root-mean-square error (RMSE) was 3.58 kg/m^3 during the calibration period and 3.45 kg/m^3 during the validation period. This represents scaled-RMSE (Barnett et al., 2012) values of 10.2% and 9.9%, respectively, indicating an acceptable level of model-measurement mismatch for the proposed application of the model, particularly given the heterogeneous nature of the island's subsurface, the high temporal dynamics and the manual approach to model calibration. There are few previous attempts at physically based simulation of island lenses with which to compare our calibration statistics. A comparable study is the modelling of Kish Island (Persian Gulf) by Ataie-Ashtiani et al. (2013), who produced a scaled-RMSE (i.e., modelled versus measured salinity) of 21%, albeit their salinity data set was considerably smaller than that available for Bonriki Island.

The initial and calibrated parameters are shown in Table 1. Hydraulic conductivity values generally increased during the calibration process, because the initial simulations underestimated concentrations (i.e., overestimated lens thickness). Significant changes to transport parameters were required to improve the simulation of the freshwater–seawater transition zone location and thickness, including a reduction in α_L to 0.8 m and an increase in porosity to 30%.

Cross-sectional depictions of the calibrated model's salinity predictions are presented in Fig. 3, with comparison to observed values. The model matches reasonably well the geometry of the freshwater lens for both the pre-abstraction (validation) period (e.g., May 1985; Fig. 3a), and after 27 years of abstraction (e.g., June 2014; Fig. 3b). The model's ability to recreate temporal salinity variations at the multi-level observation wells was an important performance criterion, given the use of the monitoring network in management decision-making. The transience of freshwater lens salinities is shown for BN27 (on cross section A-A′) and BN11 (located near galleries 16 and 17) in Fig. 8. The vertical position of the EC = 2.5, 10 and 25 mS/cm lines are represented.

Fig. 8 shows that the elevations of measured EC levels are reproduced by the model to within only a few metres, whereas the temporal trends in the elevation of EC isolines are matched reasonably well by the model. Salinity contours exhibit highly dynamic vertical movements, with displacements of > 5 m occurring annually and long-term changes of around 20 m recorded for the 2.5 mS/cm EC contour. Water-level responses to pumping and recharge over long timeframes are

Table 1
Values of initial and calibrated model parameters. Multiple values in columns 3 and 4 correspond to the respective *K*-zones listed in the second column. *K*-zones are illustrated in Fig. S2 in the EMS.

Model parameter	*K*-zones	Initial value	Calibrated value
K_H Holocene sediments, lagoon to ocean side	3, 4, 5, and 6	1.0, 5.0, 8.0, 12.0 m/d	2.5, 9.2, 16.7, 35.9 m/d
K_V Holocene sediments, lagoon to ocean side	3, 4, 5 and 6	0.2, 1.0, 1.6, 2.4 m/d	0.5, 1.8, 3.3, 7.2 m/d
K_H Top soil and surficial Holocene sediments	1	5.0 m/d	9.4 m/d
K_V Top soil and surficial Holocene sediments	1	1.0 m/d	1.9 m/d
K_H Beach rock Holocene sediments, ocean side	2	4.0 m/d	10.0 m/d
K_V Beach rock Holocene sediments, ocean side	2	0.8 m/d	2.0 m/d
K_H Fish ponds, lagoon side	Not shown in cross section	0.1 m/d	0.2 m/d
K_V Fish ponds, lagoon side	Not shown in cross section	0.02 m/d	0.04 m/d
K_H Upper Pleistocene, lagoon to ocean side	7 and 8	10.0, 16.0 m/d	30.0, 61.9 m/d
K_V Upper Pleistocene, lagoon to ocean side	7 and 8	3.5, 4.5 m/d	10.5, 17.4 m/d
K_H Lower Pleistocene	9	500.0 m/d	913.5 m/d
K_V Lower Pleistocene	9	100.0 m/d	182.7 m/d
n		0.2	0.3
α_L		12.0 m	0.8 m
α_T		0.05 m	0.04 m
α_V		0.01 m	0.008 m

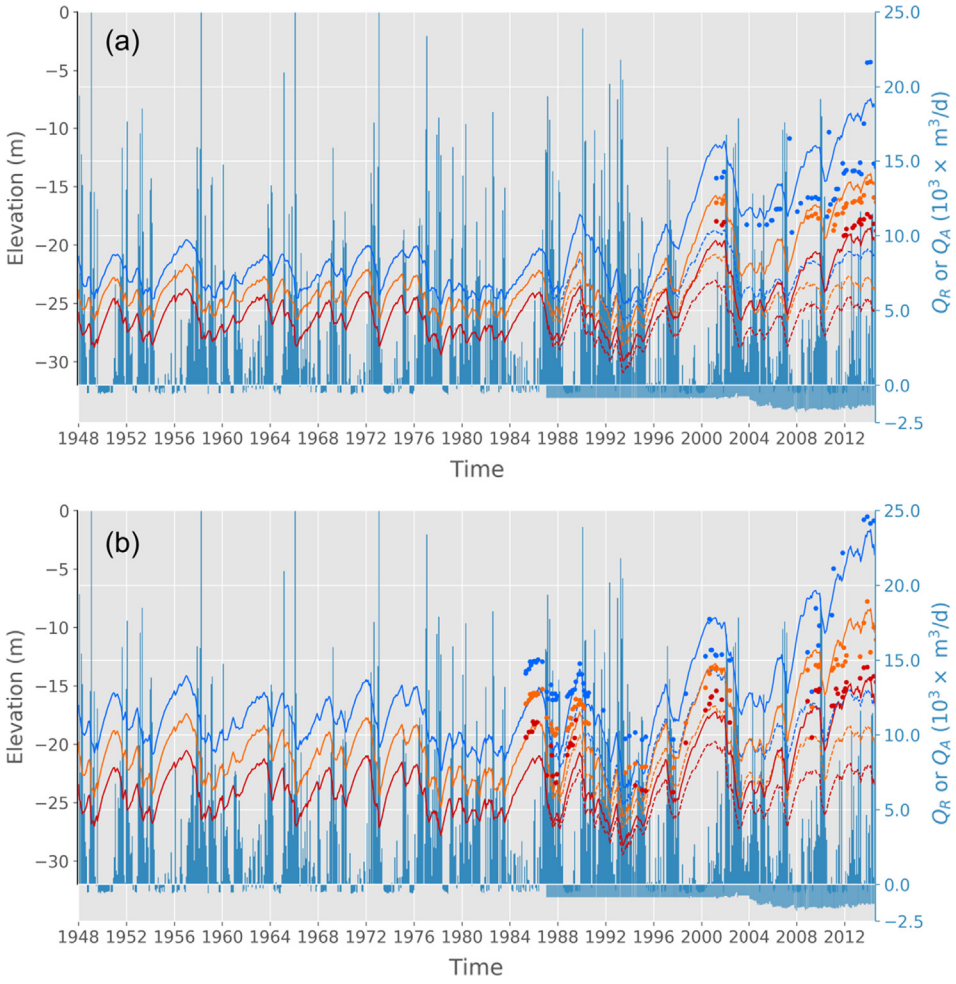

Fig. 8. Comparison of the modelled (solid lines) and measurement-based (points) vertical position of EC contour lines of 2.5, 10 and 25 mS/cm (blue, orange and red, TDS values of 1.8, 7.2 and 18 g/L, respectively) at (a) BN27 on cross section A-A′ and (b) BN13 on cross section B-B′. The dashed lines represent the model simulations without pumping. The volumetric recharge and abstraction rates are plotted as dark blue and light blue bars, respectively. Note that abstraction rates are always negative whereas recharge rates can be positive or negative. (For interpretation of the references to colour in this figure legend, the reader is referred to the web version of this article.)

masked by tidal variations, and are thus not particularly helpful for the calibration of the non-tidal model of Bonriki lens (Sinclair et al., 2015). Where water table changes have been observed, the variation tends to be < 1 m (Sinclair et al., 2015), and thus, changes to the storage of freshwater in Bonriki Island is associated more so with changes in the elevation of salinity rather than heads.

Fig. 9 illustrates measurements of the temporal variation in abstracted water EC, with comparison to flow-weighted mean EC values from the model. The model appears to be underestimating the effect of the recharge variability on the temporal changes of salinity of the abstracted water prior to 2010, but after this, variations in the pumped water salinity (i.e., at the trunk main) are closely matched by the model. This is reflected by the value of the Nash-Sutcliffe coefficient (Nash and Sutcliffe, 1970), which is −0.02 for the entire period for which EC values at the trunk main were available (March 1999 – February 2014), but 0.83 for the period since January 2010. Additional graphs, extending the results shown in Figs. 8 and 9, are included in the ESM (Figs. S3–S60) to illustrate the comparison between model outcomes and salinity measurements at observation wells and pumping galleries. In general, the same patterns as evident in the trunk main

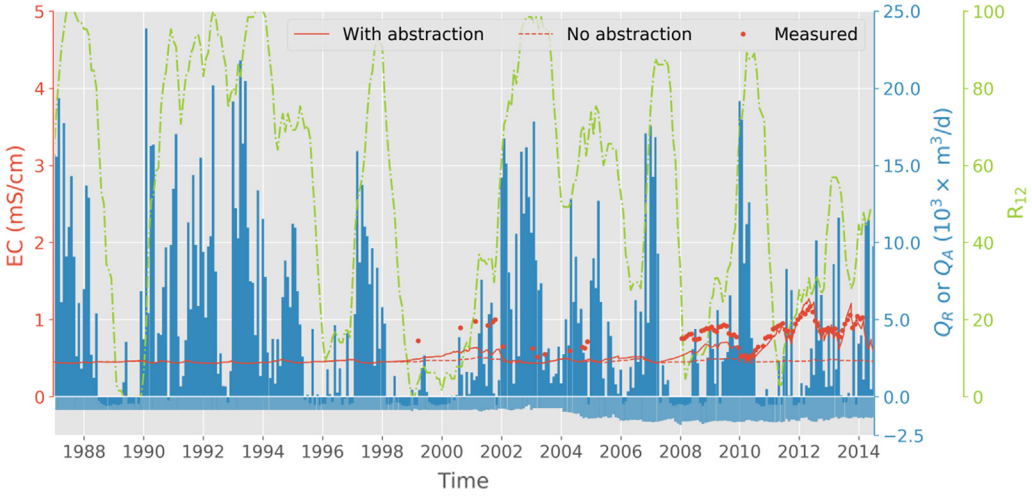

Fig. 9. Comparison of computed and measured EC values of the pumped water at the trunk main during January 1987 to June 2014. The solid and dashed red lines represent model scenarios with and without abstraction, respectively. The volumetric recharge and abstraction rates are plotted as dark blue and light blue bars, respectively. The green line represents the 12-month rainfall ranking (R_{12}; see Section 3.4). (For interpretation of the references to colour in this figure legend, the reader is referred to the web version of this article.)

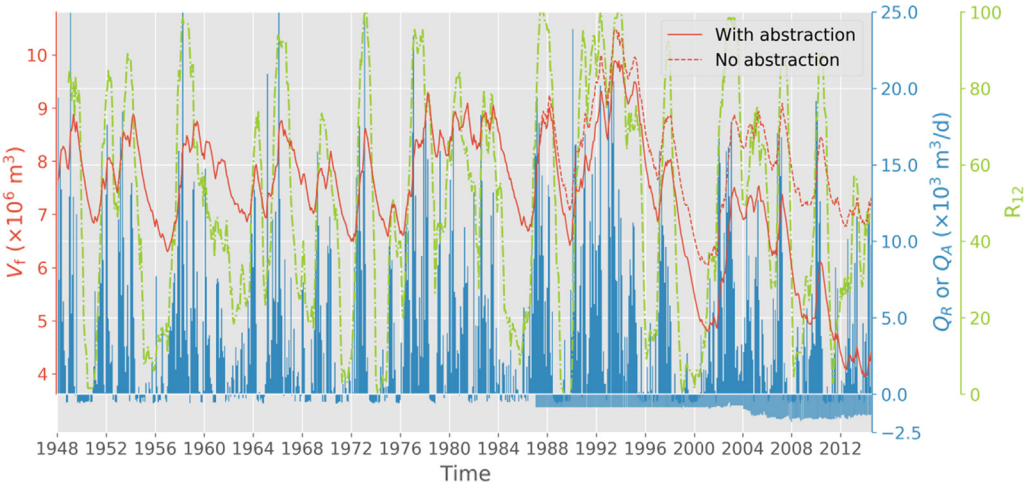

Fig. 10. Simulated freshwater volume (V_f) during the period January 1948 – June 2014. The solid red line represents the model scenario with abstraction, the dashed line is for the model with no pumping. The volumetric recharge and abstraction rates are plotted as dark blue and light blue bars, respectively. The green line represents the 12-month rainfall ranking (R_{12}). (For interpretation of the references to colour in this figure legend, the reader is referred to the web version of this article.)

(Fig. 9) are apparent for most of the individual galleries (see ESM Figs. S3–S24).

4.2. Historical trends

Fig. 10 shows the development of V_f with time for the model simulation period, superimposed on abstraction, recharge and R_{12} trends. The results demonstrate that V_f is controlled by both recharge and pumping, as expected. V_f displays temporal trends that reflect those of R_{12} for the model simulation that neglects pumping.

The impact of abstraction is especially evident during the last 10 years of the pumping simulation, when V_f shows a declining trend punctuated by short periods of partial recovery. In 2014, the volume of freshwater seems to have reached an all-time low. Within the same period, the modelled salinities at the trunk main (and at the individual galleries, see ESM Figs. S3–S24) become increasingly sensitive to dry phases, especially after 2008. These trends are consistent with the cross-sectional depictions of the lens for May 1985 and June 2014 (Fig. 3), which clearly reveal that the lens has shrunk considerably since pumping began. Climate influences on the two lens snapshots (i.e., 1985 and 2014) can be ascertained by considering respective R_{12} values. For the period May 1984 to April 1985, R_{12} ranged between 15 and 42%, while for June 2013 to May 2014, it ranged between 28 and 52%. So, while the rainfall during the one-year period before June 2014 was higher than during the year leading up to May 1985, the freshwater volume was markedly lower. The difference is therefore attributable to abstraction, consistent with the significant difference in V_f between simulations with and without abstraction (Fig. 10). In the absence of pumping, a decreasing trend in V_f is also apparent for the period 2004–2014, although the rate of decline is rather subdued, and the final value of V_f for the no pumping case is within the range of values calculated during the previous time-sequence (i.e., 1948–2004; Fig. 10).

An improved interpretation of the lens evolution is possible by plotting ΔV_f versus $V_{abs,tot}$, as given in Fig. 11. The intention here is to explore the key water-balance elements that lead to the lens reduction shown in the previous figures. Blue bars are added to Fig. 11 to indicate periods when $R_{12} > 75\%$, i.e., sequences of very high rainfall. At the onset of the pumping period (i.e., 1987), ΔV_f shows an increasing trend, which is due to the lens adjusting to the introduction of abstraction. ΔV_f subsequently falls during 1990–1995 due to above-average rainfall, despite continued abstraction throughout this time. The declining trend in ΔV_f indicates that the lens volume was being replenished following depletion during the prior period (i.e., 1987–1990). However, complete replenishment was not achieved (i.e., $\Delta V_f > 0$; Fig. 11). In the years following 1995, ΔV_f increases almost monotonically, with exception of the 2002–2004 wet period. From Fig. 11 it can also be seen that by mid-2014, when $\sim 11 \times 10^6$ m^3 of groundwater had been abstracted since 1987, ΔV_f was almost 3×10^6 m^3. This latter amount was taken from the store of freshwater that would have been available under natural conditions. The rest of the nearly 11×10^6 m^3 of abstracted groundwater represents captured freshwater discharge that would otherwise have been lost to the sea, on the basis that gross recharge to the aquifer is independent of abstraction effects in the model.

Fig. 12 presents the ΔV_f results of models with scaled abstraction rates. Fig. 12a shows ΔV_f behaviour as a function of time. As expected, lower abstraction rates lead to diminished depletion of the freshwater lens. However, the freshwater lens is not returned to its "natural condition" is any of the cases, and only the 25% scenario shows extended periods of almost stable values (i.e., independent of time) of ΔV_f after 2005. Upward trends in Fig. 12a indicate that the lens volume has not yet reached a new equilibrium condition, even where the pumping is reduced to as low as 25% of historical values. The final values of ΔV_f at the end of the simulations are displayed on the right-hand side of Fig. 12a, and as fractions of that from the calibration simulation (i.e., 2.90×10^6 m^3; Fig. 12a) equate to 70%, 43% and 20% for the 75%, 50% and 25% scaled-abstraction scenarios, respectively. This means that for reduced abstraction rates, ΔV_f is proportionally lower relative to $V_{abs,tot}$. By extension, a pumping rate at which $\Delta V_f \approx 0$ would likely be around 5% of historical pumping rates, given roughly consistent difference between $\Delta V_f/V_{abs,tot}$ (×100%) and scaled-abstraction rates, as above.

Fig. 12b is a similar graph to Fig. 11 but includes the results of models with reduced abstraction rates. The lines follow approximately similar trajectories, indicating that the gradient ($\Delta V_f/V_{abs,tot}$) is not particularly sensitive to the abstraction rate. In other words, lower rates of abstraction lead to delayed contraction of the lens, with the level of depletion being similar to that of higher abstraction rates, except at a later time. Specifically, as lens depletion appears to be mainly dependent on $V_{abs,tot}$ (Fig. 12b), scaling the abstraction rate leads to an approximately inversely proportionate delay in the timing of lens depletion (e.g., halving the abstraction rate leads to roughly doubling of the time before a particular level of lens depletion occurs). One might expect though that quasi-steady state conditions (i.e., changes in V_f in time become dependent only on changes in recharge with no further reduction due to pumping) become established for the 25% scenario before the scenarios with the higher abstraction rates, but the simulation period considered apparently was not yet long enough for this to become manifest.

Fig. 13 contains a comparison of monthly flow rates of recharge (Q_R) and net coastal discharge (Q_{coast}) for the entire model. Q_R represents the integrated recharge through the top of the model domain, while Q_{coast} is the integrated, net inflow through specified-head cells representing the ocean and lagoon floors. Negative values of Q_{coast} indicate that fresh groundwater is discharging to the ocean and lagoon

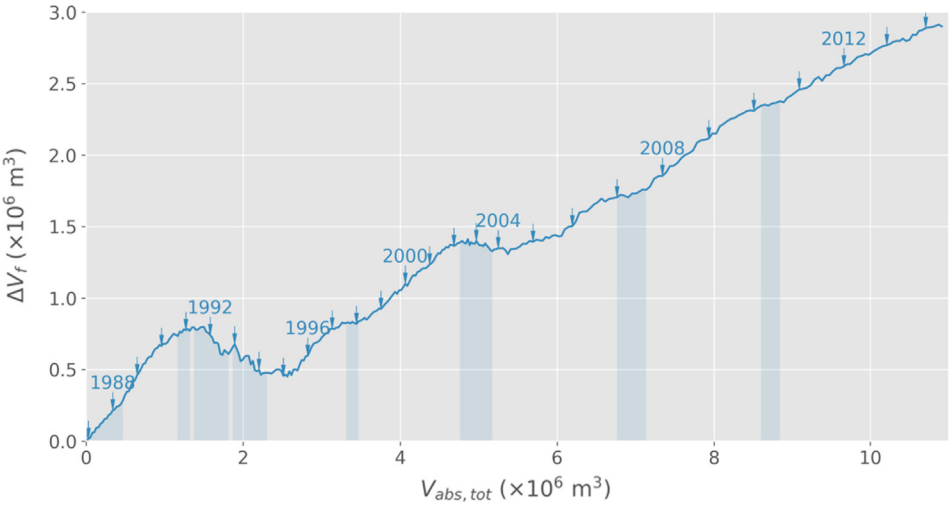

Fig. 11. Graph showing the pumping-induced depletion of the lens (ΔV_f) plotted against the total volume of pumped groundwater ($V_{abs,tot}$). The blue bars in the figure indicate periods when $R_{12} > 75\%$, i.e., periods of very high rainfall. The blue arrows mark the start of years. (For interpretation of the references to colour in this figure legend, the reader is referred to the web version of this article.)

(i.e., submarine groundwater discharge (SGD) exceeds seawater influx to the aquifer), whereas positive values indicate that SGD is less than the seawater influx, and therefore the aquifer is accumulating seawater. The colour of the data points reflects the value of $\Delta V'_f$ (positive values indicate lens growth) in accordance with the scale of the colour bar.

The general downward-sloping trend of the data points in Fig. 13 shows that the outflow to the lagoon and ocean is high when recharge is high, as expected for the small size and high permeability of Bonriki Island. Conversely, when recharge is low, there is the possibility of significant net inflows of seawater to the aquifer (i.e., positive Q_{coast} events), more so when abstraction is included in the model (compare Fig. 13a and b). The relatively narrow band of data points around the 1:1 line suggests that (a) the rate of net seaward discharge is closely linked to recharge rates, and (b) Q_{coast} and recharge trends are approximately concomitant, because significant time-lags would be expected to widen the data cluster. Data points above the 1:1 line in Fig. 13 indicate that net discharge to the sea is less than net recharge (i.e., $-Q_{coast} < Q_R$), whereas data points below the 1:1 line identify periods when net seaward discharge exceeds recharge (i.e., $-Q_{coast} > Q_R$). The former situation tends to occur more so under the highest recharge rates (i.e., as a result of freshwater lens growth) and when abstraction is considered (i.e., seawater discharge is reduced by pumping). The latter situation (i.e., $-Q_{coast} > Q_R$) is more prevalent in the absence of abstraction and during low recharge periods, because these conditions (particularly in combination) are associated with SGD that persists during periods of low rainfall through losses to the lens' freshwater storage. Both situations are associated with time lags between recharge events and responses in SGD.

Periods of lens contraction, indicated by yellow-to-red symbols (i.e., $\Delta V'_f < 0$) in Fig. 13, occur predominantly under conditions of net outflow through the coastal boundary ($Q_{coast} < 0$). That is, despite that net recharge exceeds extraction, causing coastal outflow of freshwater, the lens declines. Most of the yellow symbols in Fig. 13a (i.e., $\Delta V'_f = 0$) occur at Q_R values of around 2500 m^3/d (i.e., a flux of 1.7 mm/d based on the island's area of ~1.47 km^2), whereas in Fig. 13b they occur mostly around 4000 m^3/d (2.7 mm/d). The difference between these numbers is roughly equal to the mean abstraction rate since 2006. Moreover, under conditions of no abstraction, positive values of Q_{coast} occur only when $Q_R < 0$, whereas with abstraction this becomes when $Q_R < 1500$ m^3/d, approximately. This is the intuitive consequence of less SGD or more seawater intrusion under the abstraction regime than under no-abstraction conditions, for the same amount of recharge. We can also interpret from this that recharge rates of approximately 2500 m^3/d plus the total rate of pumping are required for stable lens conditions on Bonriki Island. Inspection of Figs. 8–10 show that recharge commonly falls below this threshold for significant periods of time over the available rainfall record, leading to lens contractions that are further evident from increases in measured (and modelled) EC

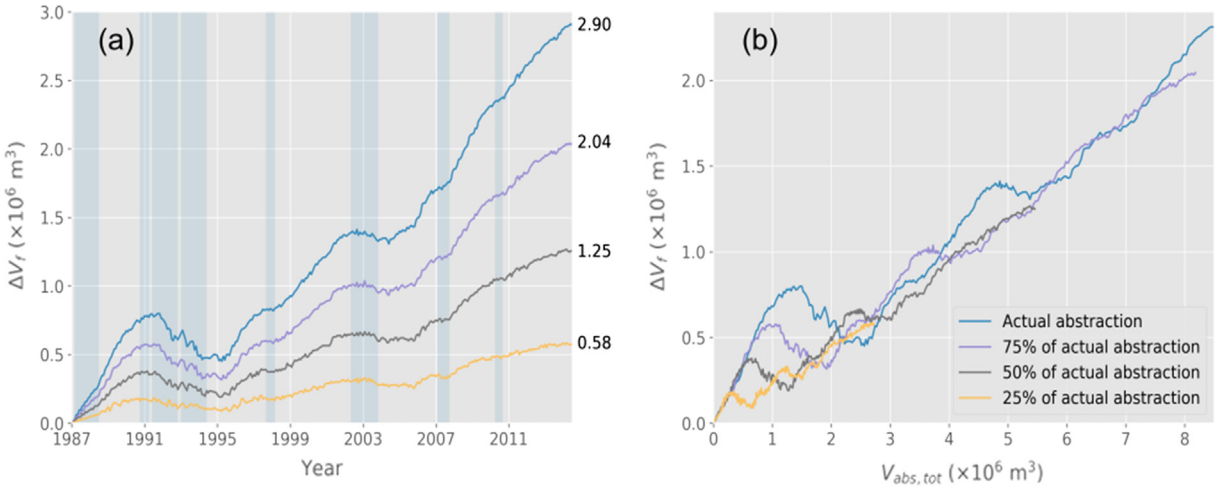

Fig. 12. Trends in ΔV_f for different abstraction rates, plotted as a function of (a) time and (b) $V_{abs,tot}$. The percentages shown in the legend represent the fraction of abstraction (relative to the calibrated model) used in modified-pumping simulations. Note vertical scale differences. The blue bars in the left figure indicate periods when $R_{12} > 75\%$. (For interpretation of the references to colour in this figure legend, the reader is referred to the web version of this article.)

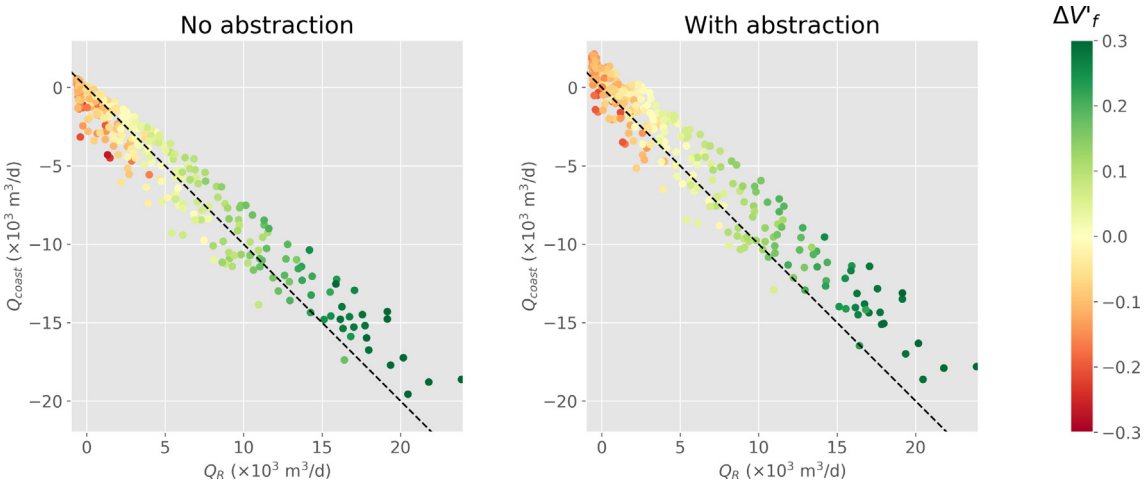

Fig. 13. Graphs showing the net flow rate of groundwater across the coastal boundary (Q_{coast}) plotted against the net volumetric recharge rate (Q_R) for the model (a) without abstraction and (b) with abstraction. Marker symbol colours indicate $\Delta V'_f$ ($\times 10^6$ m^3). Positive values of Q_{coast} indicate that seawater inflows exceed SGD, and positive values of $\Delta V'_f$ represent periods of lens growth.

values (Fig. 10).

5. Discussion

The strong dependency of Bonriki Island's freshwater volume and the pumped water salinity on recharge rates are in accordance with findings from other freshwater lens systems on atoll islands (Bailey et al., 2014; Van der Velde et al., 2006). This temporal variability is captured reasonably well by the numerical model, albeit our assessment of the calibration fit is largely subjective. The calibration result and the use of model input parameters that fall within expected values lead us to conclude that the model is an adequate tool for exploring lens behaviour, including under various abstraction scenarios. Our application of the model provides new insights into the lens that are important for both management decision-making and for understanding the physical processes that occur within atoll island settings. For example, the importance of pumping is evident from the comparison between model simulations with and without abstraction wells. This adds to previous studies of pumping impacts that adopt similar strategies except using density-independent groundwater models (e.g., Knowling et al., 2015). Indeed, climate drivers alone are unable to explain the lens thinning and shallow groundwater salinity increases that have become apparent in the field data over the last two decades. Therefore, trends of lens contraction are primarily caused by the exploitation of fresh groundwater, and not by changing recharge conditions.

The numerical model presented here is comparable to that of the freshwater lens on Home Island of the South Keeling atoll by Ghassemi et al. (2000) in terms of hydrogeological conditions, spatial scale and data availability. Ghassemi et al. (2000) stated that their "modelling exercise failed" and, although they did not did not define criteria for calibration success, they concluded "calibration could not be achieved", which they attributed to the karstic nature of the system. They did not show the differences between measured and modelled concentrations for their entire dataset, so it is impossible to make a direct quantitative comparison between the performance of the Bonriki model and their model. Yet, although the Bonriki model also shows some significant deviations between the measured and modelled configuration of the freshwater lens at individual observation wells (see Figs. 3, 7 and 8, and ESM Figs. S25–S60), as well as for the salinities of some of the galleries (see ESM Figs. S3–S24), we contend that a more optimistic conclusion about the usefulness of numerical models to simulate freshwater lenses in atoll environments is warranted. Indeed, given the karstic nature of the system, it is unlikely that a high degree of model accuracy can be achieved no matter how comprehensive the dataset and calibration effort. Moreover, a numerical model should not be expected to be able to accurately forecast salinities at individual pumping wells, as has been found for coastal aquifer models more generally (e.g., Sanford and Pope, 2010; Werner et al., 2013). Despite such limitations though, the Bonriki model was useful in analysing long-term trends of the volume of the freshwater resource, and in distinguishing between natural and anthropogenic impacts. This ability makes the model an important instrument to support the sustainable management of water supply, and serves as a benchmark for atoll island investigation.

Under natural conditions, decreases in lens volume occur (i) during periods of low or negative recharge when the coastal discharge of freshwater exceeds net recharge, and (ii) when freshwater losses due to mixing of freshwater and seawater within the aquifer (due to hydrodynamic dispersion) exceed the difference between freshwater inflows and losses. These processes combine to create complex relationships between the volume of fresh groundwater and SGD and recharge, as demonstrated by the spread of data points representing $\Delta V'_f = 0$ in Fig. 13a. Abstraction influences the aforementioned factors controlling lens volume, potentially enhancing dispersive effects and raising the recharge threshold at which the lens volume can increase (as described in the previous section).

Both modelled and measured salinity trends indicate that significant increases in lens volume are apparent only when high recharge rates are sustained over periods of several months or more (Fig. 10). Surprisingly, storage increases during sustained recharge events are generally similar with or without abstraction effects, leading to a somewhat linear relationship between lens volume and $V_{abs,tot}$, which is largely independent of the abstraction rate (i.e., Fig. 12b). In a similar manner, Q_R and Q_{coast} are correlated at the one-month temporal resolution of the model (Fig. 13). This means that a large fraction of the recharge is probably lost to SGD within one month or less. This finding is consistent with that of Jocson et al. (2002), who analysed the relationship between water level and recharge for the northern Guam Lens Aquifer and argued that it was likely that high recharge rates would cause a rapid increase of the flow of groundwater to the sea.

The median ratio of the yearly volumetric abstraction rate over the yearly volumetric recharge rate during the period 2004–2014 was 36%. The median abstraction rate over the same period was 1526 m^3/d, which is below the 1660 m^3/d currently considered to be the sustainable rate (Fig. 4). Nonetheless, the Bonriki freshwater lens appears to be in a state of decline. This is apparent from the virtually linear shrinkage of the freshwater volume attributable to pumping since 2004 (Fig. 12). Cross sections showing the change in lens geometry between 1985 and 2014 (Fig. 3) support this assertion. Moreover, the salinities of the

abstracted water are becoming increasingly sensitive to droughts, as evidenced towards the end of the simulation period (Fig. 9 and ESM Figs. S3–S24). That is, the salinities rise after a series of dry months but do not completely recover to pre-drought levels during the following wet phase. In the model scenario without abstraction, the salinity of the groundwater at the location of the abstraction galleries shows hardly any variability with time (Fig. 9). These results indicate that abstraction is causing thinning of the freshwater lens. In a thick lens, the volume of freshwater varies with time as recharge conditions vary, but this hardly affects the salinities of the abstracted groundwater, as the saltwater at depth does not reach the galleries. Under the current pumping regime, however, thinning of the freshwater lens has brought saltwater closer to the galleries. Subsequently, some of the abstraction galleries collect brackish water during dry periods, causing a marked rise in salinity at specific locations. The model-calculated freshwater volumes indicate that $V_f = 4.3 \times 10^6\,m^3$ at the end of the simulation period in June 2014, whereas on average it was $V_f = 7.7 \times 10^6\,m^3$ prior to pumping in 1987, which means that almost half of the volume of freshwater ($3.4 \times 10^6\,m^3$) has been lost. This is because of mixing by hydrodynamic dispersion and a decrease of the freshwater storage by both lowering of the water table and rising salinity during periods of low recharge. As discussed in the previous section, under groundwater abstraction conditions, the recharge rate required to cause the freshwater lens to grow becomes higher than under natural conditions.

Fig. 10 provides initial evidence that supports the application of R_{12} as an approximate and informative indicator of V_f attributable to climatic conditions in the absence of pumping. This is an important finding given that lens volumes in islands and coastal areas more broadly are challenging to determine based on EC measurements, and ascertaining the climate-induced lens performance using only field data is almost impossible. Water levels are also a poor indicator of lens conditions as they do not reflect the volume of freshwater lost from an aquifer when the loss is partially compensated by seawater intrusion (Morgan et al., 2012). Moreover, the R_{12} parameter is easy to calculate if rainfall records are available and less cumbersome to implement than the time-series models by Van der Velde et al. (2006), which are based on a convolution integral that also captures the antecedent rainfall conditions but in a less intuitive way.

The results of our study indicate that lens contraction caused by abstraction is a multi-decadal process that is superimposed on natural variations, and can become almost independent of climate drivers (Figs. 11 and 12a). While under natural conditions and during the early stages of abstraction, shallow groundwater salinities and R_{12} are essentially independent, they become more strongly correlated at later times (Fig. 9). This is apparent from the intensified fluctuations of the water salinity at the trunk main (a result of the freshwater lens becoming thinner) that follow the changes of R_{12}. Therefore, we suggest caution in the use of R_{12} as a general indicator of the health of the Bonriki groundwater system under the current stressed conditions, since abstraction effects lead to relations between R_{12} and V_f as well as between R_{12} and abstraction water salinity that do not remain fixed. For management purposes, it can thus be misleading to rely on R_{12} only, because salinities of the abstracted water in a thinned lens will start to show a stronger response to climatic variations, and the evolution of these relationships unfortunately can not be easily predicted. Collecting rainfall measurements (and other weather data) is nonetheless critically important, as is taking regular salinity measurements. As this study has shown, the response times of the lens, even in permeable, small-scale lens systems like Bonriki Island, make that monitoring needs to be sustained over many decades in order to fully capture the abstraction impacts.

While the salinities of the water abstracted from the galleries appear to respond stronger to droughts during recent years, there are currently no immediate issues with the salinity of the water supply. Nevertheless, the observed trends call for a reappraisal of the management strategies of the freshwater lens. Several options could be considered. The pumping rates for individual galleries could be adjusted in such a way that those least sensitive to salinization pump more than those of which the salinity rises rapidly during dry phases. However, the long-term effects of this strategy should be investigated. Moreover, given the high water usage of the deep-rooted palm trees, vegetation management could be adopted that considers the trade-off between the value of the trees for sustenance and environmental functioning, and their negative impact on the lens through evapotranspiration withdrawals. Finally and importantly, a salinity trigger-level approach is considered important in providing early warning for a management response to preserve fresh groundwater and minimise the adverse effects of seawater intrusion when there are reduced inputs of recharge. The threshold of $2500\,m^3/d$ plus abstraction, devised in this study, may serve as a management trigger in future water policy development. The current trend of lens thinning may require water saving measures and alternative sources of freshwater to be identified, which could include harvested rainwater or desalinated seawater.

6. Conclusions

This study investigated the long-term effects of pumping on a freshwater lens on an atoll island (Bonriki Island, Tarawa Atoll, Kiribati). Based on a comprehensive data set of meteorological, geological and groundwater data, a numerical model was constructed which was used to infer the development of the freshwater volume and the water balance components for the island between 1 January 1948 and 30 June 2014. Abstraction was simulated during the last 27.5 years of the simulation (i.e., since 1 January 1987).

The results clearly show that under natural conditions, the freshwater volume is subject to significant changes that are driven by the rainfall intensity. By comparing model simulations with and without abstraction, the effect of abstraction could be isolated from these natural variations in freshwater volume. This showed that abstraction causes sustained contraction of the lens over the 27.5 years of pumping considered in this study. The rate of decline of the freshwater volume did not show abatement over time, which means that the freshwater volume has not yet reached a new equilibrium with respect to the pumping stresses. This is the case even for hypothetical, scaled-abstraction scenarios, where the pumping is reduced as low as 25% of historical values. Our finding that lens adjustment to the abstraction stresses spans a period of nearly three decades means that numerical simulations for the assessment of sustainable yield must be based on timescales of several decades even for small and permeable islands like Bonriki Island.

The efforts to monitor groundwater and abstraction water salinities over several decades have been proven essential in assessing the state of the freshwater resource. Reliance on drought indices like the R_{12} used on Tarawa is appropriate under unstressed conditions or for low abstraction rates. But as thinning of the lens continues and shallow groundwater salinities become more variable with time, the relationship between R_{12} and abstraction water salinity is no longer fixed. Caution is therefore required to rely on such indicators to assess the health of the freshwater reserve. Because of its size and rainfall rates, the Bonriki freshwater lens is relatively resilient compared to other islands and this thus holds in particular for smaller islands with less recharge. Further work has to focus on management options for groundwater abstraction on Bonriki Island and a re-evaluation of the appropriate sustainable yield. Amongst a range of options, trigger-level approaches based on salinity must be considered, which will be the subject of future studies.

Acknowledgements

This study resulted from the partnership between two projects: the Bonriki Inundation Vulnerability Assessment (BIVA) project from the Australian government's Pacific–Australia Climate Change Science and

Adaptation Planning Program (PACCSAP), part of the International Climate Change Adaptation Initiative, and the Climate and Abstraction Impacts on Atoll environments (CAIA) project, financed by the European Union (EU) and implemented by the African Caribbean and Pacific Group of States (ACP) and the Pacific Community (SPC). Adrian Werner is supported by the Australian Research Council's Future Fellowship scheme (project number FT150100403). We thank the Australian Government and the EU for funding, staff of PUB and MPWU, Kiribati, for their help with field work and data contribution, Anthony Falkland and Ian White for technical expertise provided during the course of the projects, the Water and Sanitation programme of the Geoscience, Energy and Maritime Division at SPC for support, and our colleagues who worked with us.

Appendix A. Supplementary data

Supplementary data associated with this article can be found, in the online version, at https://doi.org/10.1016/j.jhydrol.2018.06.015.

References

AGDHC, 1982. Kiribati – Tarawa Water Resources Pre-Design Study. Australian Government Department of Housing and Construction, Canberra, Australia.

Alam, K., Falkland, A., Mueller, N., 2002. Sustainable Yield of Bonriki and Buota Freshwater Lenses, SAPHE Project, Hydrogeology Component, Tarawa, Kiribati.

Allen, D.M., Holding, S., Foster, S., Hsieh, A., Larocque, I., Klassen, J., Van Pelt, S., Gurdak, J., Taniguchi, M., 2014. Assessment of SIDS Groundwater Systems, Transboundary Water Assessment Programme, Final Report, submitted to UNESCO-IHP, 44 p.

Ataie-Ashtiani, B., Rajab, M.M., Ketabchi, H., 2013. Inverse modelling for freshwater lens in small islands: Kish Island, Persian Gulf. Hydrol. Process. 27, 2759–2773. https://doi.org/10.1002/hyp.9411.

Australian Bureau of Meteorology and CSIRO, 2011. Chapter 6: Kiribati. In: Climate Change in the Pacific: Scientific Assessment and New Research, Volume 2: Country Reports, pp. 93-110, ISBN: 9780643107137, www.pacificclimatechangescience.org/wp-content/uploads/2013/09/Volume-2-country-reports.pdf.

Bailey, R.T., Jenson, J.W., Olsen, A.E., 2010. Estimating the ground water resources of atoll islands. Water 2, 1–27. https://doi.org/10.3390/w2010001.

Bailey, R.T., Khalil, A., Chatikavanij, V., 2014. Estimating transient freshwater lens dynamics for atoll islands of the Maldives. J. Hydrol. 515 (Supplement C), 247–256. https://doi.org/10.1016/j.jhydrol.2014.04.060.

Barnett, B., Townley, L.R., Post, V., Evans, R.E., Hunt, R.J., Peeters, L., Richardson, S., Werner, A.D., Knapton, A., Boronkay, A., 2012. Australian groundwater modelling guidelines. Waterlines Report No. 82, National Water Commission, Canberra, Australia, 203 p., ISBN: 978-1-921853-91-3.

Bosserelle, A., Jakovovic, D., Post, V., Rodriguez, S.G., Werner, A., Sinclair, P., 2015. Bonriki Inundation Vulnerability Assessment (BIVA) Assessment of sea-level rise and inundation effects on Bonriki Freshwater Lens, Tarawa Kiribati – Groundwater Modelling report. SPC Technical Report SPC00010, 167 p.

Burgess, S.M., 1987. The climate and weather of Western Kiribati. New Zealand Meteorological Service, Publication 188(7), Wellington, New Zealand, 44 p., ISSN 0110-6937, http://docs.niwa.co.nz/library/public/nzmsmp188-7.pdf.

Comte, J.-C., Join, J.-L., Banton, O., Nicolini, E., 2014. Modelling the response of fresh groundwater to climate and vegetation changes in coral islands. Hydrogeol. J. 22 (8), 1905–1920. https://doi.org/10.1007/s10040-014-1160-y.

Dunham, R.J., 1962. Classification of carbonate rocks according to depositional texture. In: W.E. Ham (Ed.), Classification of Carbonate Rocks – A Symposium, American Association of Petroleum Geologists Memoir 1, Tulsa, USA, pp. 108–121.

Falkland, A., 1991. Hydrology and Water Resources of Small Islands: A Practical Guide. A contribution to the International Hydrological Programme, Paris, France: United Nations Educational, Scientific and Cultural Organization, 453 p.

Falkland, A.C., 1992. Review of Tarawa Freshwater Lenses, Republic of Kiribati. Australian International Development Assistance Bureau, Report No. HWR 92/682, Canberra Australia, 73 p.

Falkland, A.C., Woodroffe, C.D., 2004. Chapter 19 – Geology and hydrogeology of Tarawa and Christmas Island, Kiribati. In: Vacher, H.L., Quinn, T.M. (Eds.), Developments in Sedimentology. Elsevier, pp. 577–610. https://doi.org/10.1016/S0070-4571(04)80041-4.

Galvis-Rodriguez, S., Post, V., Werner, A., Sinclair, P., 2017. Climate and Abstraction Impacts in Atoll Environments (CAIA): Sustainable management of the Bonriki Water Reserve, Tarawa, Kiribati. Pacific Community (SPC) Technical Report SPC00054, Suva, Fiji, 142 p., ISBN: 978-982-00-1061-1.

Ghassemi, F., Alam, K., Howard, K., 2000. Fresh-water lenses and practical limitations of their three-dimensional simulation. Hydrogeol. J. 8 (5), 521–537. https://doi.org/10.1007/s100400000087.

Griggs, J.E., Peterson, F.L., 1993. Ground-water flow dynamics and development strategies at the atoll scale. Ground Water 31 (2), 209–220. https://doi.org/10.1111/j.1745-6584.1993.tb01813.x.

Holding, S., Allen, D.M., 2015. From days to decades: numerical modelling of freshwater lens response to climate change stressors on small low-lying islands. Hydrol. Earth System Sci. 19, 933–949. https://doi.org/10.5194/hess-19-933-2015.

Illangasekare, T., Tyler, S.W., Clement, T.P., Villholth, K., Perera, A.P.G.R.L., Obeysekera, J., Gunatilaka, A., Panabokke, C.R., Hyndman, D., Cunningham, K.J., Kaluarachchi, J.J., Yeh, W.W.-G., van Genuchten, M.T., Jensen, K., 2006. Impacts of the 2004 tsunami on groundwater resources in Sri Lanka. Water Resour. Res. 42, W05201. https://doi.org/10.1029/2006WR004876.

Jacobson, G., Taylor, F.J., 1981. Hydrogeology of Tarawa Atoll, Kiribati. Bureau of Mineral Resources Record No. 1981/31, Australian Government, Canberra, Australia.

Jocson, J.M.U., Jenson, J.W., Contractor, D.N., 2002. Recharge and aquifer response: Northern Guam Lens Aquifer, Guam, Mariana Islands. J. Hydrol. 260 (1), 231–254. https://doi.org/10.1016/S0022-1694(01)00617-5.

Jones, B., Ng, K.C., Hunter, I.G., 2004. Chapter 8 – Geology and hydrogeology of the Cayman Islands. In: Vacher, H.L., Quinn, T.M. (Eds.), Developments in Sedimentology. Elsevier, pp. 299–326. https://doi.org/10.1016/S0070-4571(04)80030-X.

Knowling, M.J., Werner, A.D., Herckenrath, D., 2015. Quantifying climate and pumping contributions to aquifer depletion using a highly parameterised groundwater model: Uley South Basin (South Australia). J. Hydrol. 523, 515–530. https://doi.org/10.1016/j.jhydrol.2015.01.081.

KNSO, 2016. 2015 Population and Housing Census, Volume 1: Management Report and Basic Tables, Kiribati National Statistics Office, Bairiki, Kiribati, 197 p., http://www.mfed.gov.ki/statistics/documents/2015_Population_Census_Report_Volume_1final_211016.pdf.

Langevin, C.D., Thorne Jr., D.T., Dausman, A.M., Sukop, M.C., Guo, W., 2008. SEAWAT version 4: a computer program for simulation of multi-species solute and heat transport. Techniques and Methods Book 6, Chapter A22, U.S. Geological Survey, Reston, 39 p.

Liu, C.W., Lin, C.N., Jang, C.S., Chen, C.P., Chang, J.F., Fan, C.C., Lou, K.H., 2006. Sustainable groundwater management in Kinmen Island. Hydrol. Process. 20, 4363–4372. https://doi.org/10.1002/hyp.6171.

Loco, A., 2017. Climate and Abstraction Impacts in Atoll Environments (CAIA): Flow meter testing, Buota and Bonriki Water Reserves, Tarawa, Kiribati. Pacific Community (SPC) Technical Report SPC00050, Suva, Fiji, 142 p., ISBN: 978-982-00-1057-4.

Mather, J., 1973. The groundwater resources of Southern Tarawa, Gilbert and Ellice Islands. Hydrogeological Department, Institute of Geological Sciences, London, UK, 54 p.

Morgan, L.K., Werner, A.D., Simmons, C.T., 2012. On the interpretation of coastal aquifer water level trends and water balances: a precautionary note. J. Hydrol. 470, 280–288. https://doi.org/10.1016/j.jhydrol.2012.09.001.

Nash, J.E., Sutcliffe, J.V., 1970. River flow forecasting through conceptual models. Part I: A discussion of principles. J. Hydrol. 10, 282–290.

Sanford, W.E., Pope, J.P., 2010. Current challenges using models to forecast seawater intrusion: lessons from the Eastern Shore of Virginia, USA. Hydrogeol. J. 18 (1), 73–93. https://doi.org/10.1007/s10040-009-0513-4.

Sinclair, P., Singh, A., Leze, J., Bosserelle, A., Loco, A., Mataio, M., Bwatio, E., Galvis Rodriguez, S., 2015. Groundwater Field Investigations, Bonriki Water Reserve, South Tarawa, Kiribati. Bonriki Inundation Vulnerability Assessment (BIVA) Project, Secretariat of the Pacific Community (SPC), Technical Report SPC00009, Suva, Fiji, 267 p.

Stewart, G., Walker, K., Fontaine, K., Dixon-Jain, P., Norman, R., 2014. Pacific Island Groundwater Vulnerability to Future Climates Dataset. Geoscience Australia, Canberra. http://www.ga.gov.au/metadata-gateway/metadata/record/gcat_81575.

Underwood, M.R., Peterson, F.L., Voss, C.I., 1992. Groundwater lens dynamics of atoll islands. Water Resour. Res. 28, 2889–2902. https://doi.org/10.1029/92WR01723.

UNESCO, 2016. Small Island Developing States – UNESCO's Action Plan, Ikhlef, K, Nakashima, D. (Eds), United Nations Educational, Scientific and Cultural Organization, Paris, France, 32 p.

Vacher, H.L., 2004. Introduction: Varieties of carbonate islands and a historical perspective. In: Vacher, H.L., Quinn, T.M. (Eds.), Developments in Sedimentology. Elsevier, pp. 1–33. https://doi.org/10.1016/S0070-4571(04)80021-9.

Van der Velde, M., Javaux, M., Vanclooster, M., Clothier, B.E., 2006. El Niño-Southern Oscillation determines the salinity of the freshwater lens under a coral atoll in the Pacific Ocean. Geophys. Res. Lett. 33 (21), L21403. https://doi.org/10.1029/2006GL027748.

Van der Velde, M., Vakasiuola, M., Green, S.R., Manu, V.T., Minonesi, V., Vanclooster, M., Clothier, B.E., 2007. Climatic variation, recharge and freshwater lens salinity of a coral atoll in the Pacific Ocean, A New Focus on Groundwater–Seawater Interactions. In: Proceedings of Symposium HS1001 at IUGG2007, Perugia, Italy, pp. 244–255.

Van Loon, A.F., Van Lanen, H.A.J., 2013. Making the distinction between water scarcity and drought using an observation-modeling framework. Water Resour. Res. 49 (3), 1483–1502. https://doi.org/10.1002/wrcr.20147.

Wagner, W.K., 1977. Fresh water resources on Christmas and Butaritari Islands and Southern Tarawa, Gilbert Islands, South Pacific. ESCAP Regional Mineral Resources Development Centre, Advisory services report HG 11, 43 p.

Werner, A.D., Bakker, M., Post, V.E.A., Vandenbohede, A., Lu, C., Ataie-Ashtiani, B., Simmons, C.T., Barry, D.A., 2013. Seawater intrusion processes, investigation and management: recent advances and future challenges. Adv. Water Resour. 51, 3–26. https://doi.org/10.1016/j.advwatres.2012.03.004.

Werner, A.D., Sharp, H.K., Galvis, S.C., Post, V.E.A., Sinclair, P., 2017. Hydrogeology and management of freshwater lenses on atoll islands: review of current knowledge and research needs. J. Hydrol. 551, 819–844. https://doi.org/10.1016/j.jhydrol.2017.02.047.

White, I., Falkland, A., 2010. Management of freshwater lenses on small Pacific islands. Hydrogeol. J. 18, 227–246. https://doi.org/10.1007/s10040-009-0525-0.

White, I., Falkland, T., 2012. Practical Responses to Climate Change: Developing National Water Policy and Implementation Plans for Pacific Small island Countries. In: Proceedings, Water and Climate: Policy Implementation Challenges, Practical Responses to Climate Change, 1-3 May 2012, Engineers Australia, Canberra, pp. 1–3.

White, I., Falkland, A., Etuati, B., Metai, E., Metutera, T., 2002. Recharge of Fresh Groundwater Lenses: Field Study, Tarawa Atoll, Kiribati. In: J.S. Gladwell (Ed.), Proceedings, Second International Colloquium on Hydrology and Water Resources Management in the Humid Tropics, UNESCO-IHP and CATHALAC, 22-25 March 1999, Panama City, Panama.

White, I., Falkland, T., Perez, P., Dray, A., Metutera, T., Metai, E., Overmars, M., 2007. Challenges in freshwater management of low coral atolls. J. Cleaner Prod. 15, 1522–1528. https://doi.org/10.1016/j.jclepro.2006.07.051.

White, I., Falkland, T., Rebgetz, M., 2008. Report on the protection and management of water reserves, South Tarawa, Preparation of Water Master Plan for Tarawa, KAPII Component 3, Freshwater Resources, Project 3.2.1, AusAID Grant No. TF056115, Canberra, Australia, 33 p.

Woodroffe, C.D., Falkland, T., 2004. Geology and hydrogeology of the Cocos (Keeling) Islands. In: Vacher, H.L., Quinn, T.M. (Eds.), Developments in Sedimentology. Elsevier, pp. 885–908. https://doi.org/10.1016/S0070-4571(04)80053-0.